https://doi.org/10.5194/egusphere-2026-4755
Preprint. Discussion started: 1 September 2026

Extreme hazard cyclones – concept and ERA5 climatology

Sven Voigt[1], Hanin Binder[1], Seraphine Hauser[1], and Heini Wernli[1]

[1]Institute for Atmospheric and Climate Science, ETH Zurich, Zurich, Switzerland

Correspondence: Sven Voigt (sven.voigt@env.ethz.ch)

Abstract. Extratropical cyclones shape much of the weather variability outside the tropics and can be associated with extreme precipitation and damaging winds with potentially substantial socioeconomic impacts. Consequently, identifying and understanding the cyclone characteristics associated with widespread weather extremes along their tracks is essential. This study uses 75 years of ERA5 reanalyses to characterize "cyclone extremeness" by quantifying the occurrence of extreme precipitation and surface winds along cyclone tracks. We do this by linking precipitation and 10 m wind speed extremes (values exceeding the local climatological 99.9$^{\text{th}}$ percentile) to individual cyclones and quantify the number of extremes associated with each cyclone along its track on a global scale. Extremes are considered at two time scales, 1 hour and 3 days, reflecting that the impact of an extreme surface weather event may vary with its duration. An "extreme hazard cyclone" is then defined as a cyclone that accumulates a large number of precipitation and/or wind extremes along its track. Compared to all cyclones on average, extreme hazard cyclones form at lower latitudes and are deeper, larger in cyclone area, longer-lived, and more rapidly intensifying. Most of the top 100 extreme hazard cyclones globally form in the tropics and undergo extratropical transition. When restricting the ranking to cyclones producing extremes in the North Atlantic storm track, the top 100 extreme hazard cyclones predominantly occur in summer and autumn for precipitation extremes (including extratropical transition events) and mainly in winter for wind extremes. Extreme wind hazard cyclones typically form in strongly baroclinic environments at the left exit of intense upper-level jets. In contrast, extreme precipitation hazard cyclones are slightly less deep and form in weaker baroclinic environments, but they develop a prominent vertically coherent potential vorticity tower indicative of strong diabatic processes. At the time a precipitation or wind extreme occurs, extreme hazard cyclones are generally classified as 'symmetric' in the classical cyclone phase space and those linked to many wind extremes exhibit a 'shallow warm core'. Long-duration extremes are associated either with more stationary cyclones or with cyclone clustering, both of which keep the affected region under cyclonic influence for an extended period, whereas short-duration extremes are linked to more intense and rapidly moving cyclones. The concept of extreme hazard cyclones, as introduced in this study, reveals key characteristics of cyclones associated with many precipitation or wind extremes along their track, and it provides a framework to investigate how climate change influences cyclone-driven surface weather extremes. The concept can easily be applied to specific regions of interest and extended to study cyclone impacts by including particular fields of exposure.

https://doi.org/10.5194/egusphere-2026-4755
Preprint. Discussion started: 1 September 2026

1 Introduction

Most of the daily weather in the extratropics is driven by the passage of extratropical cyclones, which transport moisture, energy, and momentum and often bring precipitation and strong winds to the regions they traverse. A majority of precipitation in the extratropics is directly linked to extratropical cyclones, both over continents and within the storm tracks (Hawcroft et al., 2012). In the Northern Hemisphere storm tracks, cyclones account for up to 90% of the total precipitation, largely in the form of frontal precipitation (Catto et al., 2012; Catto and Pfahl, 2013). The total amount of precipitation in a cyclone depends not only on moisture availability and supply, but also on the intensity of the cyclone (e.g., Field and Wood, 2007; Rudeva and Gulev, 2011; Pfahl and Sprenger, 2016). Thus, intense cyclones play a dominant role in driving extreme precipitation. Pfahl and Wernli (2012) quantified that a large fraction of precipitation extremes (defined in their study as events exceeding the 99th percentile of six-hourly accumulated precipitation) are linked to the passage of an extratropical cyclones, also in regions outside of the main storm tracks. In the mid-latitudes, these extremes are often linked to warm conveyor belts (e.g., Pfahl et al., 2014; Catto et al., 2015). Over the ocean and over flat terrain, they typically occur near the cyclone center, however, in regions with complex topography, extremes may also result from an interplay between the cyclone's circulation and the orientation of the terrain, such that the cyclone can be located farther from the location of the precipitation extreme (Pfahl, 2014).

Extratropical cyclones are also often associated with strong winds. In Europe and over the North Atlantic, cyclones bringing the strongest winds tend to form during long-lasting positive phases of the North Atlantic Oscillation, when a strong zonally oriented jet stream steers them towards the continent (Donat et al., 2010; Hanley and Caballero, 2012). The strongest surface winds can be induced by different airstreams and occur in separate areas of the cyclone (Hewson and Neu, 2015). Focusing on Europe, several studies have identified regions where wind extremes are most likely to occur in a cyclone, namely in the warm sector inflow region of the warm conveyor belt (Parton et al., 2010), in the cold jet related to the cold conveyor belt along the bent-back front (Eisenstein et al., 2023), in the cold sector influenced by dry intrusions (Raveh-Rubin, 2017), along the cold front associated with frontal convection (Earl et al., 2017), and in sting jets near the bent-back front (e.g., Browning, 2004; Clark and Gray, 2018). Which airstream contributes most to wind extremes appears to depend on the cyclone's geographic location. For instance, over western and central Europe, the strongest surface winds occur within the cold conveyor belt and cold frontal convection, whereas over eastern Europe they are strongest in the cold sector (Eisenstein et al., 2023).

Given the importance of cyclones for causing extreme surface weather, they can have a substantial socioeconomic impact in the affected regions. The development of a set of infamous storms and their severe impact have been described extensively in detailed case studies (e.g., Salmon and Smith, 1980; Gyakum, 1983; Hoskins and Berrisford, 1988; Wernli et al., 2002; Fink et al., 2009; Liberato et al., 2013; Riboldi et al., 2026). Several of these high-impact cyclones were characterized by rapid intensification, typically measured by the maximum 24-h decrease of minimum sea level pressure (SLP) along the cyclone track. Intense latent heating – fueled by the condensation of abundant water vapor – is essential for rapid cyclone intensification (e.g., Kuo and Reed, 1988; Wernli and Gray, 2024). Consequently, these systems occur most frequently over the oceans, where the moisture supply is greatest (Roebber, 1984). This is reflected in the more equatorward cyclogenesis of cyclones related to surface extremes, identified by Pfahl and Wernli (2012) for systems causing heavy precipitation in the storm tracks and over

https://doi.org/10.5194/egusphere-2026-4755
Preprint. Discussion started: 1 September 2026

the east of the continents, and by Bentley et al. (2019) for cyclones with anomalously strong winds over central and eastern North America, which allows these cyclones to access a larger moisture supply.

Part of that equatorward shift of cyclones associated with surface extremes compared to the overall cyclone climatology may also stem from tropical cyclones that re-intensify as extratropical systems. Tropical cyclones are more likely to undergo extratropical transition and make landfall as intense extratropical systems if baroclinicity is large, if they get influenced by an intense upper-level trough as they recurve, or if they cross a strong jet stream (e.g., Klein et al., 2000; Hart et al., 2006; Keller et al., 2019; Sainsbury et al., 2022). Climatological studies have shown that roughly half of the tropical cyclones in the North Atlantic and western North Pacific transition to extratropical systems and may cause extreme weather when making landfall (Pezza and Simmonds, 2008; Bieli et al., 2019; Sainsbury et al., 2020).

As some cyclones generate particularly severe wind and precipitation hazards, characterizing this specific class of systems and their relationship to surface weather extremes is critically important. "Cyclone extremeness" can be assessed in a variety of ways, and several approaches exist to identify the most extreme systems. In this study, we choose a pragmatic approach that aims at focusing on surface weather extremes: We link local extremes of precipitation and 10 m wind speed to individual cyclones and quantify the number of surface weather extremes associated with each cyclone along its track. We then define an "extreme hazard cyclone" as a cyclone that accumulates a large number of extremes in either precipitation or wind speed (or both) during its lifetime. Related approaches were used in studies by Klawa and Ulbrich (2003), Leckebusch et al. (2007), and Little et al. (2023), which integrated a so-called storm loss index along cyclone tracks over central and northern Europe. In contrast to these studies, we quantify the occurrence of local wind and precipitation extremes along cyclone tracks on a global scale, and we consider multiple time scales for local weather extremes ranging from one hour to three days. Including extremes of different durations reflects the idea that the impact of an extreme surface weather event varies with its duration. For instance, short-duration precipitation extremes may produce flash floods in urban areas or small catchments, while long-duration extremes are more likely to drive large-scale, long duration flooding (e.g., Marchi et al., 2010; Breugem et al., 2020). Correspondingly, a 1-h surface wind extreme can cause structural damage to buildings, whereas 3-day wind extremes may result in prolonged shutdowns of wind energy facilities. Identifying extreme hazard cyclones associated with the largest number of surface weather extremes in each of the four categories (precipitation vs. wind, short vs. long duration) enables a comparison of their characteristics and to study how they differ from climatological (i.e., "normal") cyclones. Therefore, this study aims to answer the following questions:

1. Which cyclones accumulate the largest number of precipitation and 10 m wind speed extremes along their track? How do they compare to climatology in terms of their genesis location, size, intensity, intensification, thermal or potential vorticity (PV) structure?

2. When and where do these cyclones form? Is there a preferred season for their occurrence?

3. Do cyclones associated with a large number of precipitation extremes show different properties than cyclones linked to many wind extremes?

https://doi.org/10.5194/egusphere-2026-4755
Preprint. Discussion started: 1 September 2026

4. Do cyclones linked to short-duration extremes show other characteristics than cyclones associated with longer-duration extremes?

The remainder of the paper is organized as follows: Sect. 2 describes the data and the attribution of extreme precipitation and surface winds to individual cyclones used in this study. Section 3 presents a case study of Hurricane Igor, followed by an examination of the tracks and seasonality of the 100 cyclones accumulating the largest number of precipitation and surface wind extremes globally. In Sect. 4, we focus on the most extreme cyclones in the North Atlantic, investigating their track properties alongside cyclone-relative composites and their thermal structure. Section 5 finally summarizes our main findings and addresses potential caveats.

2 Data and methods

2.1 ERA5

This study is based on the ERA5 reanalysis dataset provided by the European Centre for Medium-Range Weather Forecasts (ECMWF; Hersbach et al., 2020), using data from March 1950 to March 2025. The hourly data are originally available at a spectral resolution of T639 on 137 vertical levels, but interpolated data on a $0.5° \times 0.5°$ horizontal grid were used for this study. ERA5 is a multi-decadal and fairly high-resolution global dataset constrained by all available observations, produced with a numerical model and data assimilation scheme, and therefore constitutes the ideal basis for addressing the research questions posed above.

2.2 Cyclone detection and tracking

Surface cyclones and tracks are obtained from SLP fields following the method by Wernli and Schwierz (2006), with refinements described in Sprenger et al. (2017). The algorithm detects a cyclone center as a local SLP minimum, encompassed by closed SLP contours in increments of $0.5\,\mathrm{hPa}$. The area enclosed by the outermost closed contour is identified as the surface cyclone (note that this area typically varies along the cyclone track) and used to construct a binary cyclone mask indicating cyclone presence at each grid point. Cyclone tracks are computed by linking cyclone centers between consecutive time steps. Based on the previous movement of a cyclone, its center at the next time step is estimated. The closest corresponding SLP minimum within a search radius is then considered the continuation of the track (see Sprenger et al. (2017) for more details about the tracking).

Accurately tracking cyclone centers over complex topography and for shallow systems remains challenging for many algorithms (Neu et al., 2013), sometimes resulting in large, and therefore unrealistic, jumps between consecutive time steps. To prevent such artifacts and the erroneous linking of unrelated SLP minima, tracks exhibiting propagation speeds exceeding $200\,\mathrm{km\,h^{-1}}$ were therefore split at the time of unrealistic propagation[1] and treated as separate cyclones. By restricting the

[1] As a benchmark we considered the track of the exceptionally fast-moving Storm Lothar (Wernli et al., 2002), which reached a maximum propagation speed of $180\,\mathrm{km\,h^{-1}}$.

https://doi.org/10.5194/egusphere-2026-4755
Preprint. Discussion started: 1 September 2026

analysis to cyclones with a lifetime of at least 24 h, we further exclude short-lived systems and short fragments of separated tracks.

2.3 Surface extremes and their attribution to cyclones

We focus on local weather extremes in precipitation and 10 m wind speed, defined as events exceeding the 99.9th percentile, following a similar percentile-based approach as for instance used in Pfahl (2014) but adopting a higher percentile threshold. Percentiles are calculated across the entire dataset (March 1950 - March 2025) and separately at each grid point. Extreme events are identified on timescales of 1 h and 72 h. For the 72-h window, wind speeds are averaged and precipitation is accumulated from the hourly data. The approach results in a maximum of 657 events per type of extreme at each grid point. These events may occur consecutively, i.e., as part of the same event, or, in the case of 72-h extremes, may partially overlap. For brevity, the four types of extremes will be referred to in the following as P1 and P72 for precipitation, and W1 and W72 for 10 m wind speed, respectively.

Extreme events are linked to cyclones using the cyclone masks. Figure 1 shows the attribution of extreme events to Storm Dennis, a deep cyclone with a minimum core SLP of 934.1 hPa impacting northern Europe in February 2020 (e.g., Davies et al., 2021; Jardine et al., 2023). For each identified extreme with a duration of 1 h, we determine whether its location falls within the cyclone mask at any time along the cyclone track; events that do are linked to the corresponding cyclone (Fig. 1a). A 72-h event is attributed to the cyclone if the hourly cyclone mask overlaps the event's location at least once during the duration of the extreme (Fig. 1b). Consequently, a single long-duration event may be associated with several cyclones. To avoid counting consecutive or temporally overlapping extremes at the same grid point as separate events, the number of extremes per grid point attributed to a cyclone is limited to one per type of extreme. If multiple events of the same type of extremes at one grid point are attributed to the same cyclone, only the event with the largest magnitude is retained. Using this approach, not every identified extreme is necessarily linked to a cyclone. In particular, precipitation extremes along elongated fronts may fall outside the cyclone mask and therefore remain unattributed (Fig. 1a). However, since according to previous studies the majority of heavy precipitation events occur near the cyclone center along the warm or the bent-back front (e.g., Field and Wood, 2007; Catto and Pfahl, 2013), we expect to only miss a small fraction of cyclone-related extremes. This is shown exemplarily for Storm Dennis in Fig. 1, which illustrates that the method both captures the short-duration extremes along the warm and bent-back front around the time of maximum intensity of the cyclone, but also the long-duration extremes, which are mainly related to the mature and decay phase of Storm Dennis as it moved into the Irminger Sea towards Iceland.

For each cyclone, we then evaluate the number of local extremes of a certain type accumulated within the cyclone area along its track, weighted by the latitude of each event. As a result, each cyclone is associated with a four-dimensional hazard vector, representing the number of extremes of each type it is linked to. Cyclones are subsequently ranked according to the number of attributed extremes, yielding a list of the most extreme cyclones in terms of each type of surface hazard. This ranking can be applied globally, within a specific region, or even at the scale of a single grid point. When considering a larger geographic area, the highest ranked cyclones are not necessarily causing the most extreme precipitation or surface winds at any individual grid point, but rather are the ones with the broadest spatial hazard pattern and potential for damage.

https://doi.org/10.5194/egusphere-2026-4755
Preprint. Discussion started: 1 September 2026

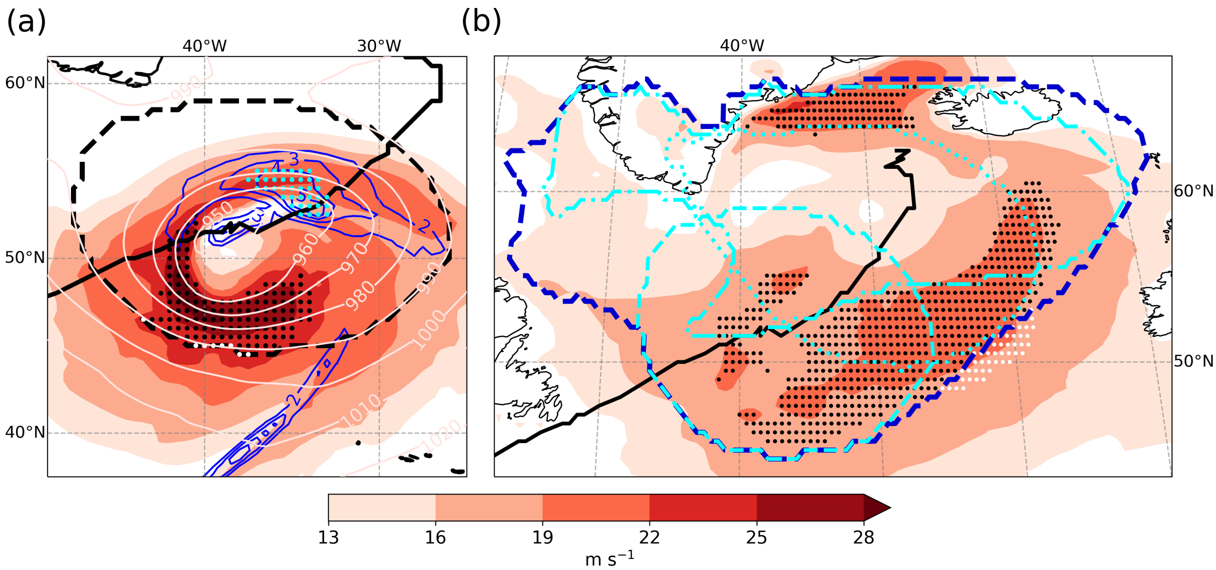

Figure 1. Example to illustrate the association of short-duration (1 h) and long-duration (72 h) surface weather extremes with individual cyclone tracks for Storm Dennis. **(a)** Shading shows 1-h wind speed at 10 m, blue contours show 1-h accumulated precipitation with a contour interval of 1 mm starting at 2 mm, and pale pink contours depict SLP in hPa at 09 UTC on 13 February 2020. The cyclone mask is shown by dashed black contours. Black and cyan dots mark W1 and P1 events linked to the cyclone, respectively, while white dots indicate W1 extremes not linked to a cyclone. **(b)** Shading shows the average 10 m wind speed over the 72-h period from 09 UTC on 13 February to 09 UTC on 16 February. Dashed, dotted, and dash-dotted cyan contours indicate the cyclone mask at 09 UTC on 13 February, at 12 UTC on the same day, and on 09 UTC on 14 February, respectively, while the dark blue dashed contour shows the envelope area covered by the cyclone mask at any time during the 72-h period. Black dots indicate W72 extremes associated with the cyclone, while white dots mark W72 extremes not linked to a cyclone. The track of Storm Dennis is shown as a solid black line.

2.4 Cyclone phase space

We also characterize the thermal and physical structure of cyclones using the cyclone phase space (CPS) developed by Hart (2003), which classifies cyclones throughout their life cycle according to their symmetry and the thermal wind in the upper and lower troposphere, respectively. The symmetry B is quantified as the difference in 900–600 hPa geopotential thickness within a 500 km radius around the cyclone center, comparing the mean on the left and right sides relative to the direction of the cyclone's motion. The thermal wind is used as a measure for the thermal structure and evaluated in two vertical segments ranging from 900 to 600 hPa ($-V_T^L$) and from 600 to 300 hPa ($-V_T^U$). The phase space of B, $-V_T^L$ and $-V_T^U$ is then typically used to classify cyclones as frontal ($B > 10\,\mathrm{m}$) or non-frontal ($B < 10\,\mathrm{m}$) and according to their thermal structure as deep warm core ($-V_T^L > 0$ and $-V_T^U > 0$), deep cold core ($-V_T^L < 0$ and $-V_T^U < 0$), or hybrid ($-V_T^L > 0$ and $-V_T^U < 0$) systems. Based on these metrics, the CPS has been shown to be useful to differentiate tropical and extratropical cyclones and to identify systems undergoing extratropical transition (e.g., Evans and Hart, 2003; Kitabatake, 2011; Wood and Ritchie, 2014; Bieli et al., 2019). In this study, we compute the three CPS parameters along all tracked cyclones.

3 Extreme hazard cyclones globally

Before extending the analysis to all cyclones globally, we first examine Hurricane Igor, which underwent extratropical transition, as an illustrative case study to demonstrate the methodology and to provide an intuition on how extremes accumulate along a cyclone track. We select Igor because it ranks among the most extreme hazard cyclones, being first for P1 extremes, and it is linked to precipitation and wind extremes along its entire track.

3.1 Case study of Hurricane Igor in September 2010

Igor developed as a tropical cyclone in early September 2010, impacting Cape Verde, and became a category IV hurricane on 12 September. It affected Bermuda on 20 September before transitioning into an extratropical cyclone. The extratropical transition and impacts associated with Igor, especially those in Newfoundland where heavy rainfall resulted in flash floods and strong winds damaged power lines and buildings, were comprehensively studied by Masson (2014).

Figure 2a shows the track of the cyclone and the associated P1 and W1 extremes. Igor had a total lifetime of 490 h and was linked to extreme events along nearly its entire track. During its early phase as a westward-propagating tropical cyclone, these were primarily P1 extremes, while the first W1 extremes developed around day four of its lifetime. During its mature tropical phase, both P1 and W1 extremes are located within the cyclone area, with W1 extremes extending farther from the storm center than P1 extremes. During the second phase of Igor's life cycle, after its transition to an extratropical cyclone, P1 extremes occur primarily northwest of the cyclone center, while W1 extremes still cover large portions of the system around the center. As the cyclone begins to weaken over the Labrador Sea, P1 extremes are found mainly over the ocean, whereas southern Greenland and Newfoundland experience wind extremes.

The absolute area of Igor covered by extreme events, along with the cyclone's minimum SLP, is shown in Fig. 2b. P1 extremes begin to occur earlier in the cyclone's lifetime than W1 extremes, with the P1-affected area being larger for the first 115 h. As Igor intensifies and its minimum SLP decreases, the area affected by W1 extremes increases rapidly, peaking at $6.5 \cdot 10^5\,\mathrm{km}^2$ one hour before the cyclone reaches its minimum SLP of 940.6 hPa. A secondary peak in W1 extreme area occurs as Igor re-intensifies in the extratropics and its SLP decreases again. Later, as the system weakens, comparatively few W1 extremes remain linked to the cyclone. The area covered by P1 extremes similarly follows a two-peaked trajectory, initially increasing to a local maximum just prior to minimum SLP before temporarily declining and reaching its overall peak during the deepening phase in the extratropics with $2.6 \cdot 10^5\,\mathrm{km}^2$ affected by P1 extremes.

Surface wind speeds and precipitation at distinct times during the cyclone's life cycle (see vertical dashed lines in Fig. 2b) are shown in Fig. 2c to Fig. 2i. Figure 2c shows the cyclone as a tropical depression a few hours before passing Cape Verde. Although winds and precipitation were still relatively weak in absolute terms, a small number of extremes already occurred close to the cyclone center. Igor then developed into a tropical storm, with wind extremes shifting to the north of the center

https://doi.org/10.5194/egusphere-2026-4755
Preprint. Discussion started: 1 September 2026

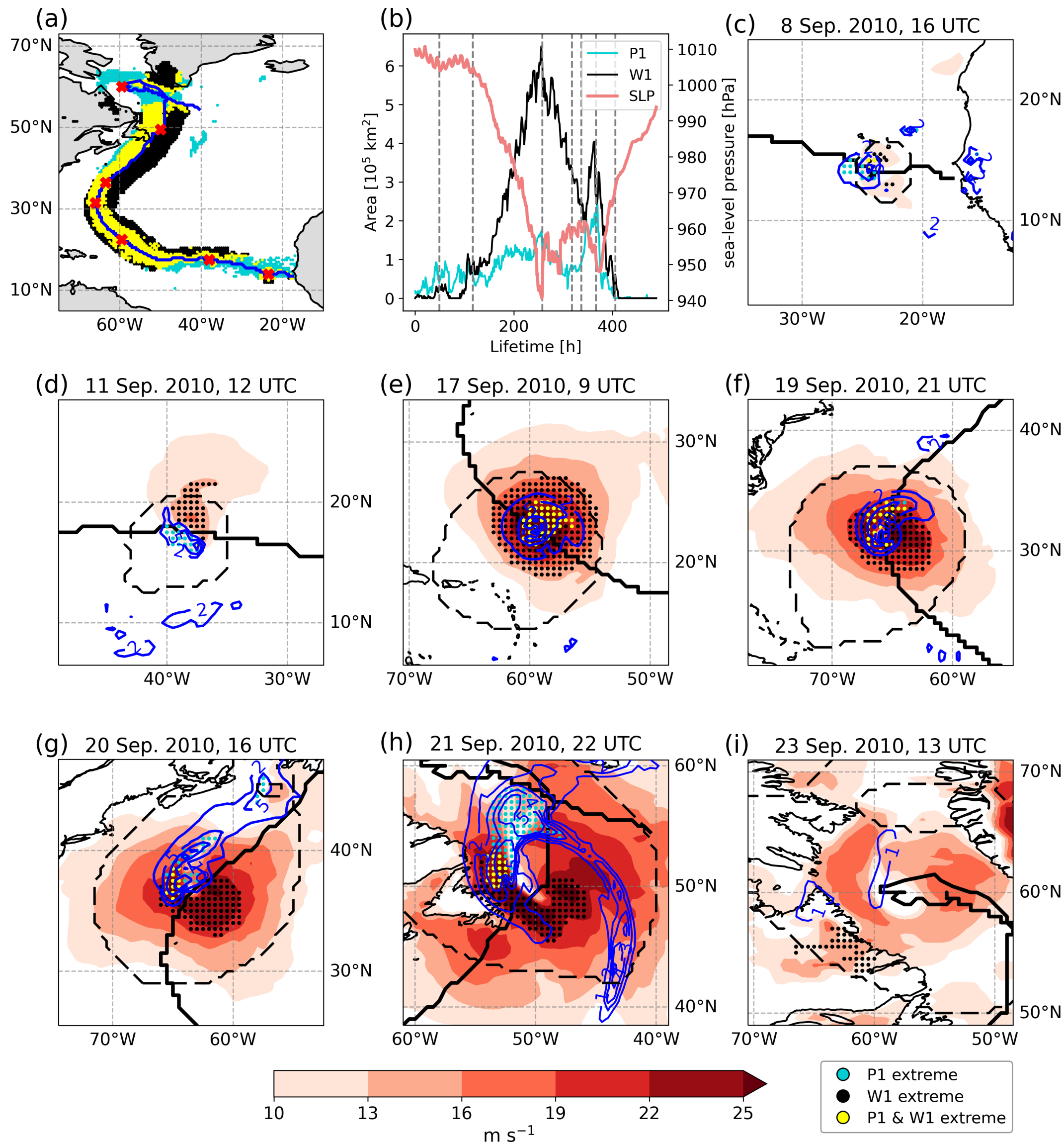

Figure 2. Case study of surface weather extremes along the track of Hurricane Igor in September 2010. In all panels, W1 extremes are shown as black dots, P1 extremes as turquoise dots, and locations with co-occurring P1 and W1 extremes as yellow dots. Thick black lines indicate the cyclone track. **(a)** Overview on W1 and P1 extremes along Igor's life cycle from the African west coast to the Labrador Sea. Red crosses mark Igor's position in panels (c-i). **(b)** Time series along the cyclone track of the absolute area of Igor exhibiting extremes in P1 (turquoise, left axis) and W1 (black, left axis), together with minimum SLP (coral, right axis). Dashed gray vertical lines indicate the times corresponding to panels **(c-i)**. (c-i) – their exact times are given on top of the panels – show Igor (c) as a tropical depression, (d) deepening tropical storm, (e) category IV hurricane, (f) at its westernmost point before recurving, (g) when starting to develop extratropical features, (h) as an extratropical cyclone, and (i) during decay. Wind speed is shown by red shading and precipitation with dark blue contours (contour interval of 1 mm). Dashed black contours mark the cyclone mask used to link extremes to the cyclone.

https://doi.org/10.5194/egusphere-2026-4755
Preprint. Discussion started: 1 September 2026

(Fig. 2d), and later intensified into a hurricane, with widespread wind extremes forming a ring around the center and precipitation extremes concentrated near the center (Fig. 2e). Igor then began moving more northward, increasing in size, but without causing any P1 or W1 extremes over the Caribbean Isles (Fig. 2e). Upon reaching Bermuda, the cyclone recurved towards the northeast and weakened slightly (Fig. 2f), before starting the transition to an extratropical cyclone. At this stage, W1 extremes were primarily located south of the cyclone center, while P1 extremes occurred in an elongated precipitation band along the bent-back front (Fig. 2g). Igor fully developed into a deep extratropical cyclone before reaching Newfoundland (Fig. 2h), exhibiting clearly visible frontal precipitation and P1 extremes along the bent-back front. The cyclone subsequently weakened but maintained large areas of strong surface winds, before finally starting to decay, while still causing strong winds and W1 extremes in Newfoundland (Fig. 2i).

This case study of Igor illustrates that extreme hazard cyclones can cause both precipitation and wind extremes along their entire track, not only during the period of maximum intensity. We also see that during the tropical phase, extremes are roughly symmetric and circular around the cyclone center, whereas during the extratropical phase, precipitation extremes tend to shift to the north of the cyclone center. Additionally, the area affected by extremes evolves throughout the cyclone's life cycle. Precipitation extremes here developed earlier than wind extremes and occupied a smaller portion of the system, while the area covered by wind extremes peaked later and covered much larger areas as the cyclone intensified and expanded in size.

3.2 The global top 100 extreme hazard cyclones

Having illustrated the extremes-to-cyclone attribution for Hurricane Igor, we now extend this analysis to all cyclones globally. Accumulating extreme events within the cyclone area along all tracks provides an objective identification of the most extreme hazard cyclones across four types of surface weather extremes. This section focuses on the 100 most extreme hazard cyclones in the categories P1, P72, W1, and W72. In the following, the top 100 cyclones in each category are referred to as extreme hazard cyclones. Individual cyclones may appear among the highest ranked for several types of surface extremes. Figure 3 shows the overlap between the 100 topmost ranked cyclones in every category. We find a total of 274 different cyclones across the four top-100 lists, of which 188 are ranked in only one category. Six cyclones appear in all four categories and all of them occurred in the Pacific. These are Tropical Cyclone Pam (2015), ranked first in both the W1 and W72 categories and classified as the third most intense system in the South Pacific in terms of minimum SLP; Supertyphoon Dale (1996); Tropical Cyclone Gavin (1985); severe Tropical Cyclone Bob (1977); Typhoon Emma (1962); and an unnamed cyclone in Australia in 1956, which reached a minimum SLP of 907 hPa. There is furthermore a larger overlap of cyclones in the two wind categories, likely because cyclones that rank highest for wind extremes exhibit some of the strongest SLP gradients, which evolve comparatively slowly and produce extreme winds both on short and longer timescales. We find only one cyclone exclusively shared by the P1 and W72 categories, which occurred in Chile in 2002 shortly before the capital experienced flash floods. Table 1 shows the three highest ranked cyclones in each of the four hazard categories, the ocean basin where they developed and intensified, and selected references that discussed the cyclones or their impacts. These systems occur in the North Atlantic and North and South Pacific, in the years from 1957 to 2015, and most of them in the autumn season. Their genesis latitude is in the tropics

https://doi.org/10.5194/egusphere-2026-4755
Preprint. Discussion started: 1 September 2026

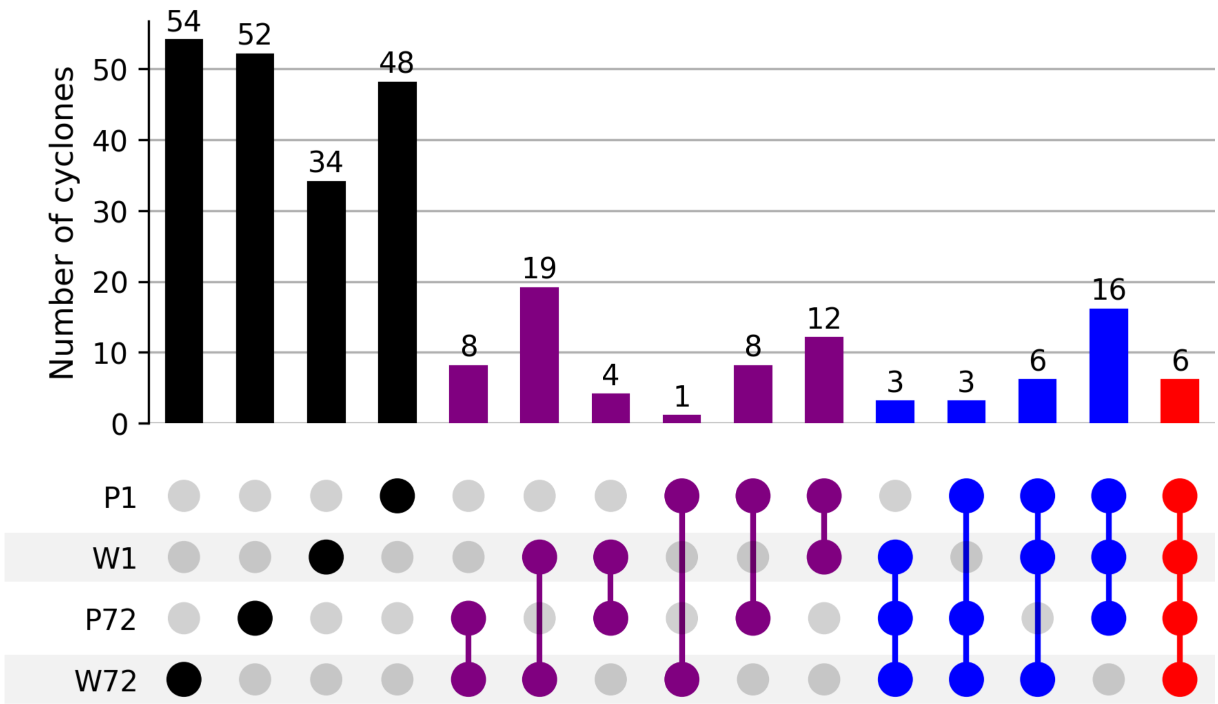

Figure 3. Overlap between the top 100 cyclones ranked by their number of associated extremes in the categories P1, W1, P72, and W72. Vertical bars indicate the number of cyclones shared between each combination of extreme categories. For example, 54 cyclones among the 100 highest ranked in every category are only extreme in W72, eight are extreme in both P72 and W72, and six are extreme in all four categories.

(not shown), but the latitude where they are associated with the largest number of extremes is variable (from about 10° to 50° latitude).

Figure 4 shows the tracks of the 100 extreme hazard cyclones in categories P1 and W1 and provides an overview of their geographical distribution and seasonal occurrence. Most of the top 100 P1 cyclones develop over the ocean (Fig. 4a), where intense latent heating and a large supply of moisture favor cyclone intensification. In the Northern Hemisphere, the number of top 100 P1 cyclones is comparable in the Atlantic and Pacific, whereas in the Southern Hemisphere, the majority form in the Indian Ocean. The selected P1 cyclones have cyclogenesis at low latitudes and form as tropical systems in all ocean basins, with the exception of the South Atlantic, where they form at relatively higher latitudes. After traversing large parts of the ocean, those originating in tropical regions often undergo extratropical transition and re-intensify as extratropical cyclones – similar to the case study of Igor (Sect. 3.1). These characteristics allow them to reach exceptionally long lifetimes of up to nearly one month and travel several thousand kilometers, accumulating a large number of P1 extremes along their tracks. Due to their tropical origin, the top 100 P1 cyclones have a pronounced seasonality and occur during boreal summer and autumn in the Northern and austral summer and autumn in the Southern Hemisphere, respectively.

https://doi.org/10.5194/egusphere-2026-4755
Preprint. Discussion started: 1 September 2026

Table 1. Information about the three top-ranked extreme hazard cyclones in the four categories, including the ocean basin where they developed and intensified, the coordinates of the cyclone center at the time of minimum SLP and at the time when they are associated with the largest number of extremes in the respective category, the cyclone type (entirely tropical [TC], entirely extratropical [ETC], or tropical cyclone undergoing extratropical transition [TC/ETC]), and selected references discussing the cyclone and its impacts.

Cyclone	Category	Ocean basin	Time	Coordinates min. SLP	Coordinates most extremes	TC/ETC	References
Igor	P1	N. Atlantic	Sep. 2010	59.5° W, 22.5° N	49.0° W, 52.5° N	TC/ETC	Han et al. (2012); Masson (2014)
Marie	P1	N. Pacific	Oct. 1972	146.5° E, 32.5° N	146.5° E, 32.5° N	TC/ETC	
Bill	P1	N. Atlantic	Aug. 2009	58.5° W, 20.0° N	27.5° W, 51.5° N	TC/ETC	Berg and Avila (2011)
Pam	W1	S. Pacific	Mar. 2015	171.0° W, 46.5° S	171.0° W, 46.5° S	TC/ETC	Nakano et al. (2017); Rey et al. (2017); Takemi (2018); Chandra and Kumar (2021)
Karen	W1	N. Pacific	Nov. 1962	132.5° E, 15.5° N	132.5° E, 15.5° N	TC/ETC	
Lola	W1	N. Pacific	Nov. 1957	149.5° E, 11.0° N	149.5° E, 11.0° N	TC/ETC	
Emma	P72	N. Pacific	Oct. 1962	151.5° E, 24.0° N	165.5° E, 38.0° N	TC/ETC	
Igor	P72	N. Atlantic	Sep. 2010	59.5° W, 22.5° N	52.0° W, 18.0° N	TC/ETC	Han et al. (2012); Masson (2014)
Tomas	P72	S. Pacific	Mar. 2010	150.5° W, 48.0° S	172.0° W, 29.5° S	TC/ETC	Taniguchi and Tajima (2020)
Pam	W72	S. Pacific	Mar. 2015	171.0° W, 46.5° S	169.5° W, 9.5° S	TC/ETC	Nakano et al. (2017); Rey et al. (2017); Takemi (2018); Chandra and Kumar (2021)
Choi-wan	W72	N. Pacific	Oct. 2015	147.5° E, 41.0° N	159.5° E, 19.0° N	TC/ETC	
Winnie	W72	N. Pacific	Aug. 1997	134.5° E, 23.0° N	150.5° E, 16.5° N	TC	Peijun et al. (2005); Zhang et al. (2005)

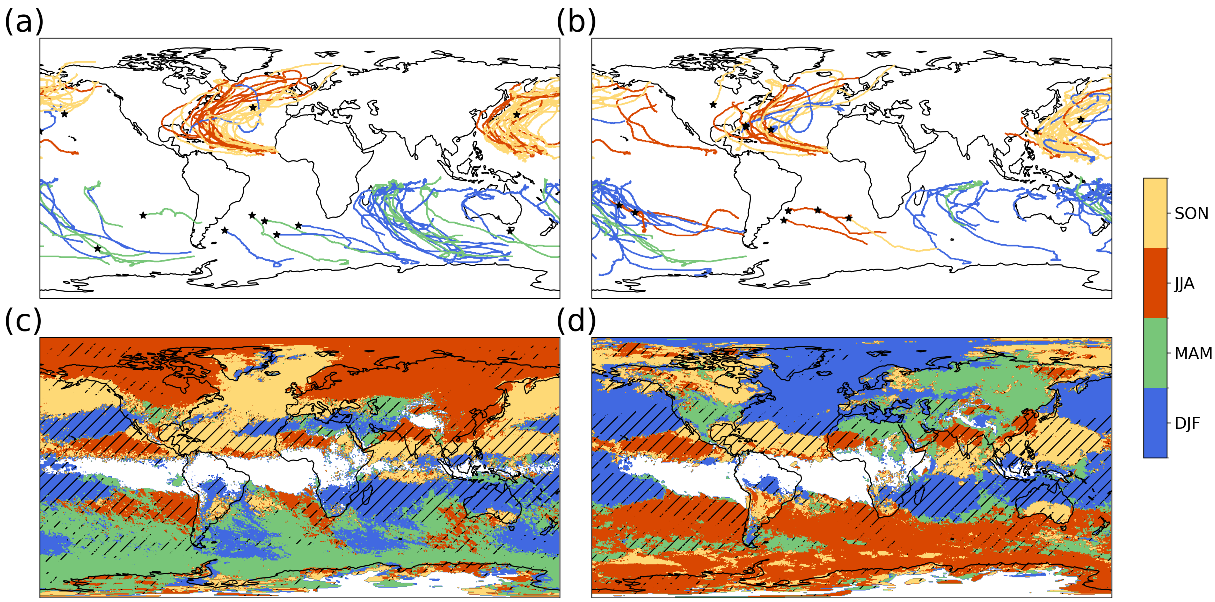

Figure 4. (a, b) Tracks of the 100 extreme hazard cyclones in the categories (a) P1 and (b) W1. Track colors indicate the season of cyclogenesis, and black stars mark cyclogenesis locations poleward of 25° latitude. **(c, d)** Seasons when the highest number of cyclone-linked extremes of (c) P1 and (d) W1 occur. Hatching indicates regions where the dominant seasons are identical for both types of extremes, and white regions show where no extremes could be attributed to cyclones.

We observe the same general patterns for the 100 W1 extreme hazard cyclones, which also tend to form at low latitudes before transitioning to extratropical systems (Fig. 4b). While the top 100 P1 cyclones show a clear seasonal pattern, the top

https://doi.org/10.5194/egusphere-2026-4755
Preprint. Discussion started: 1 September 2026

100 W1 cyclones are more variable. Some W1 systems form outside of the main tropical cyclone season of summer and autumn, particularly in the South Atlantic where a few top 100 W1 cyclones have genesis in austral winter and spring. This is accompanied by shifts in the main affected basins, with a relative increase in the top 100 W1 cyclones forming in the North Pacific and especially in the South Pacific, and fewer in the Indian Ocean, compared to the top 100 P1 cyclones.

To illustrate the seasonal distribution of extreme events, Fig. 4c, d show the season in which most cyclone-related P1 and W1 extremes occur across all cyclones (i.e., not only for the top 100 cyclones). Over the Northern Hemisphere oceans, cyclone-related P1 extremes are most frequent in boreal autumn, whereas over the continents, summer is the dominant season. In the Southern Hemisphere, cyclone-related P1 extremes occur most often over the high-latitude oceans in boreal spring, in the Indian Ocean during boreal winter, and in the subtropical southern Pacific during boreal summer. The dominant seasons for cyclone-related W1 extremes are more evenly distributed: boreal summer prevails across much of the Southern Hemisphere, boreal winter around the equator, and in the extratropical North Pacific and North Atlantic (Fig. 4d). In the tropics, the dominant seasons for P1 and W1 extremes largely coincide (hatching in Fig. 4c, d), reflecting that the same cyclonic systems often cause both types of extremes. For example, focusing on Australia, many cyclones appearing in the top 100 for P1 extremes also rank among the top 100 for W1 extremes (not shown). In extratropical regions, by contrast, the dominant seasons for cyclone-related P1 and W1 extremes generally differ, indicating that cyclones causing widespread P1 extremes are less frequently associated with widespread W1 extremes. Most top 100 P1 cyclones propagate through areas where the dominant season for extremes coincides with the season in which the cyclones develop (Fig. 4a, c). This correspondence is less consistent for the top-ranked W1 cyclones: later portions of their tracks frequently pass through regions where the local dominant season does not align with the season of the cyclone's occurrence. This does not necessarily mean that these cyclones cause 10 m wind extremes only at the beginning of their lifetimes, but rather that these systems are intense enough to also cause extremes outside the dominant season.

4 Extreme hazard cyclones in the North Atlantic

In this subsection, we apply the same approach to a smaller region and identify the systems with the largest integrated hazard along their tracks in the North Atlantic (see dashed black line in Fig. 5a). Since most of the extreme hazard cyclones identified in Sect. 3.2 originate in the tropics, we now restrict the analysis to the extratropics and consider only extremes occurring poleward of 30° N. Cyclones may have genesis and lysis outside the domain, but at least part of their area must intersect the North Atlantic box for a minimum of one time step during their lifetime for extremes to be attributed.

For each category, we analyze the 100 highest-ranked North Atlantic cyclones. We compare their characteristics both along their entire tracks and at the time when they are linked to the maximum number of extremes in their respective category. More specifically, we first investigate cyclone track properties (Sect. 4.1), then examine cyclone-relative composites of various aspects of the cyclones' structure and environmental flow to discern differences between cyclone properties across categories (Sect. 4.2), and finally analyze the cyclones' thermal structure when linked to an extreme using the cyclone phase space (Sect. 4.3).

https://doi.org/10.5194/egusphere-2026-4755
Preprint. Discussion started: 1 September 2026

4.1 Tracks of North Atlantic extreme hazard cyclones

Figure 5 shows the properties of the 100 extreme hazard cyclones in the North Atlantic. Among them, we find systems with a tropical origin transitioning to extratropical cyclones for categories P1 (Fig. 5a), W1 (Fig. 5b), and P72 (Fig. 5c), whereas the top-ranked W72 cyclones are almost exclusively originating in the extratropics (Fig. 5d). Cyclones associated with a large number of precipitation extremes predominantly develop in summer and autumn, regardless of whether they have cyclogenesis in the tropics or extratropics (Fig. 5a, c). In contrast, cyclones associated with wind extremes occur more frequently in winter, including many with genesis along the US east coast that then propagate across the Atlantic (Fig. 5b, d).

Although many of these extreme hazard cyclones have cyclogenesis outside the tropics, their genesis locations exhibit an equatorward shift relative to the climatology of North Atlantic cyclones[2] (Fig. 5e). Compared to the median climatology of 55.5° N, the median cyclogenesis latitude is between 37° N and 38.5° N for P1, W1, and P72 extreme hazard cyclones, and with 40.2° N slightly farther north for those in the W72 category. Despite a different region of interest, these findings are similar to the results of Bentley et al. (2019), who found that cyclones causing extreme weather in the US typically develop at lower latitudes than ordinary cyclones. Extreme hazard cyclones generally exhibit larger deepening rates than climatology (Fig. 5f). With a median of 1.6 and 1.8 Bergeron for P1 and W1 versus 0.8 and 1.5 Bergeron for P72 and W72, cyclones associated with short-duration extremes deepen more rapidly than those linked to long-duration extremes, and wind extremes are associated with faster-deepening cyclones than precipitation extremes of the same duration. Extreme hazard cyclones also reach much lower minimum SLP values than climatology (Fig. 5g). The lowest median minimum SLP values occur for W1 and W72 cyclones (949.9 hPa and 953.5 hPa, respectively). These values are slightly higher for P1 and P72 systems, reaching 956.2 hPa and 969.9 hPa. The median value for W1 cyclones corresponds to the 98.8^{th} percentile of the climatological distribution, while the median for P72 cyclones corresponds to only the 89.1^{st} percentile.

Lifetimes of extreme hazard cyclones tend to be much longer than those of climatological cyclones (Fig. 5h), allowing them either to travel long distances and affect large areas or to remain relatively stationary and impact a single region for an extended period. Precipitation-related extreme hazard cyclones show larger variability in lifetime than wind-related cyclones: P1 and P72 extreme hazard cyclones have median lifetimes of 128 h and 112 h, with an interquartile range of 180 h and 235 h, respectively. In contrast, W1 and W72 extreme hazard cyclones have shorter lifetimes of 102 h and 73 h with correspondingly smaller interquartile ranges of 68 h and 47 h. In addition to their longer lifetimes compared to climatology, extreme hazard cyclones are substantially larger than average cyclones, with the median of their maximum sizes approximately twice as large as the median size of a climatological cyclone (Fig. 5i). We calculated an additional metric, which is the average time a grid point is affected by the cyclone, which technically corresponds to the time the grid point is covered by the mask of the same cyclone at different times along its track. Therefore, this measure is large when cyclones are stationary (or slow-moving), long-lived, and large. The results clearly show that extreme hazard cyclones also stand out in this metric with median values ranging from 22.2 h for W72 to 24.8 h for P1 extreme hazard cyclones, equivalent to 1.7 and 1.9 times the climatological values, respectively (Fig. 5j).

[2]This climatology includes all cyclone tracks that cross the considered North Atlantic region.

https://doi.org/10.5194/egusphere-2026-4755
Preprint. Discussion started: 1 September 2026

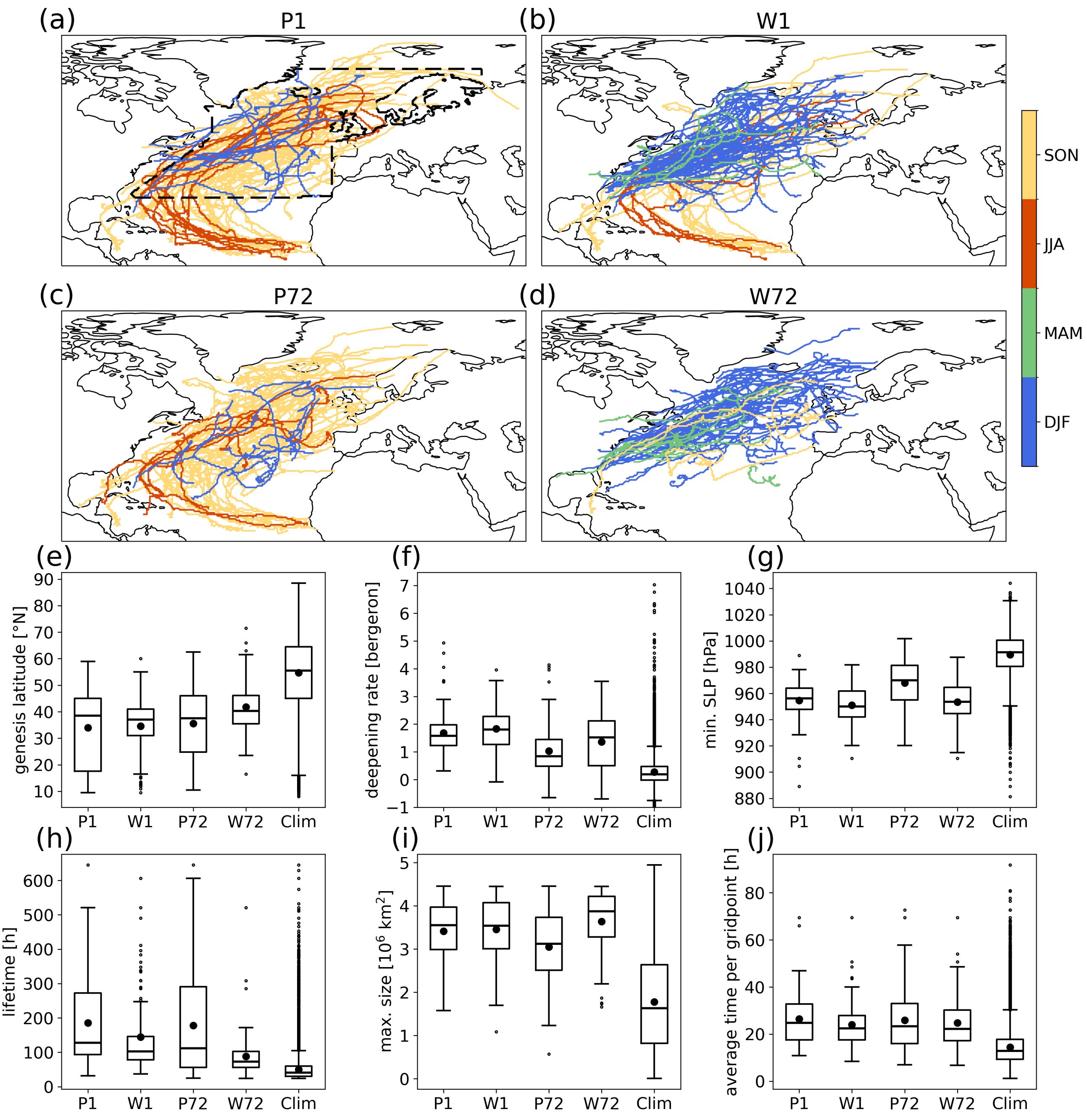

Figure 5. Tracks of the top 100 extreme hazard cyclones in the categories **(a)** P1, **(b)** W1, **(c)** P72, and **(d)** W72 in the North Atlantic, colored by the season when cyclogenesis occurred. Dashed black contours in (a) show the North Atlantic region. For these 100 cyclones as well as for the climatology, the Tukey box plots show (e) cyclogenesis latitude, (f) deepening rate, (g) minimum SLP, (h) lifetime, (i) maximum cyclone size along the tracks, and (j) average grid point residence time of cyclones. The median is shown as a horizontal line within the box plots and the mean with a thick black circle.

https://doi.org/10.5194/egusphere-2026-4755
Preprint. Discussion started: 1 September 2026

4.2 Properties of extreme hazard cyclones

Although many extreme hazard cyclones are associated with extreme events throughout their life cycle, the majority of extremes occur during the intensification phase. Rather than averaging over the entire track as in Sect. 4.1, we here focus on the properties of these cyclones in each category at the time when they are associated with the largest number of extremes. More specifically, this composite analysis investigates separately for the four categories of extreme hazard cyclones

- where the surface extremes occur relative to the cyclone center and how strong they are on average,
- the vertical structure of PV across the cyclone center at the time when the cyclones are associated with the largest number of extremes,
- the horizontal structure of upper-level PV anomalies and winds at the same time,
- and a pragmatic measure of stationarity of the cyclones.

In the following, we produce composites of the top 100 cyclones at their 'most extreme time step' for each category of extreme events. For 1-h extremes, the most extreme time step is defined as the moment when the cyclone is associated with the largest number of extreme events of that type. For 72-h extremes, we first identify the 72-hour window containing the most extremes, and then select the single time step within that window when the cyclone has the lowest central SLP value. As cyclones may move in or out of the North Atlantic region within these 72 h, we furthermore require that at least parts of the cyclone area are within the region at the most extreme time step.

4.2.1 Surface extremes relative to the cyclone center

Figure 6 shows the P1 and W1 composites for the short-duration categories and the P72 and W72 composites for the long-duration categories, together with the locations where extremes occur most frequently. In cyclones linked to many P1 extremes, strong precipitation is concentrated north of the cyclone center along the warm or the bent-back front, where the 95th percentile exceeds $11\,\mathrm{mm\,h^{-1}}$, and more variable and weaker along the cold front (Fig. 6a). Accordingly, P1 extremes are most frequently located just north of the cyclone center (hatched region in Fig. 6a). Although P1 extremes also occur along the cold front, their larger spatial variability results in no cyclone-relative region exceeding the 10% occurrence threshold used in Fig. 6 for the hatching. Similar results for the location of precipitation extremes were found by Field and Wood (2007), who composited cyclones in the North Atlantic. Catto and Pfahl (2013) also found that most extreme precipitation is associated with fronts, with the warm front contributing more extremes than the cold front. In W1 extreme hazard cyclones, precipitation is also relatively high, though less intense than in P1 extreme hazard cyclones (Fig. 6b). Similar spatial patterns are evident, with the largest values northwest of the cyclone center and lower values in the south and the east along the cold front.

The strongest surface winds in W1 extreme hazard cyclones composites are located southeast of the center and reach $22\,\mathrm{m\,s^{-1}}$, with weaker winds in the center of the system and to its north (Fig. 6c). A similar result was found in composites by Field and Wood (2007) in the North Atlantic and by Eisenstein et al. (2023) in a climatological study over Europe,

https://doi.org/10.5194/egusphere-2026-4755
Preprint. Discussion started: 1 September 2026

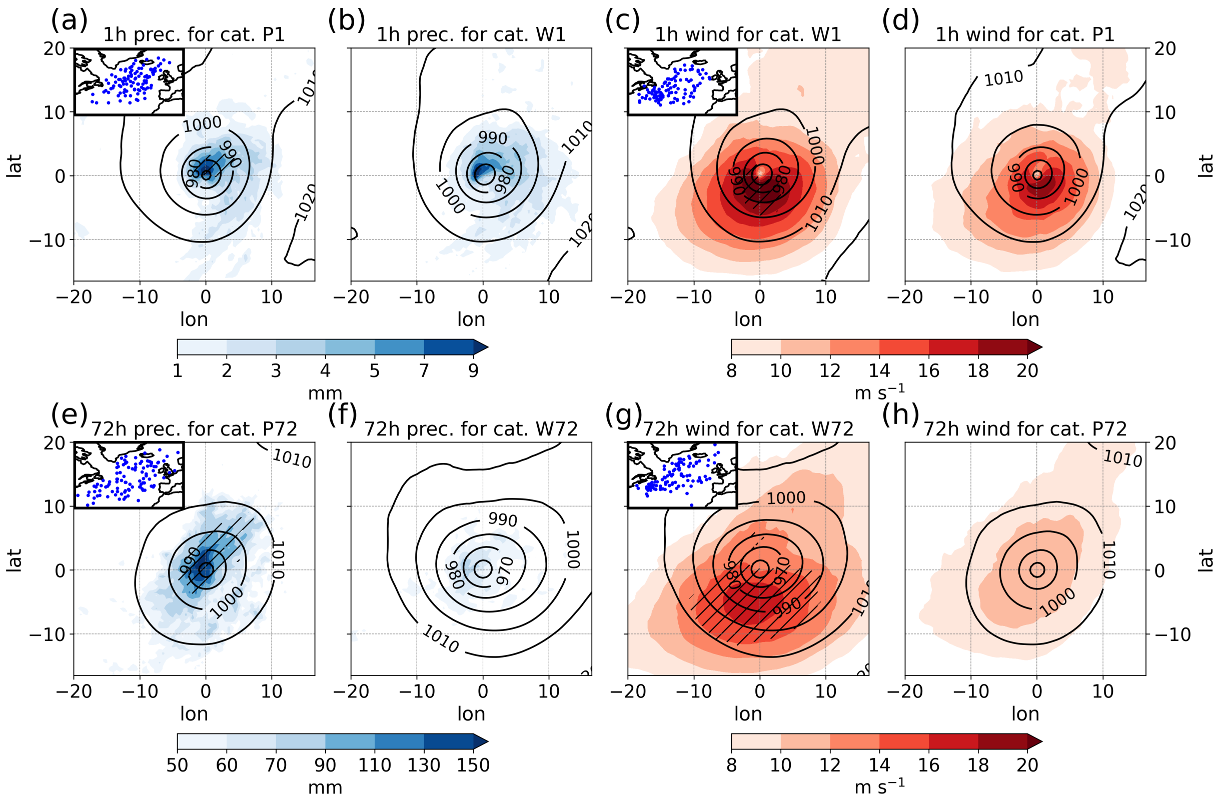

Figure 6. Cyclone-center-relative composites of precipitation and 10 m wind speed for each category of extreme hazard cyclones in the North Atlantic at the time they are linked to the largest number of extremes in the respective category. The composites show hourly precipitation for the hazard categories (a) P1 and (b) W1, instantaneous 10 m wind speed for the categories (c) P1 and (d) W1, 72-h accumulated precipitation during the 72-h window when the cyclone is linked to the highest number of extremes for the categories (e) P72 and (f) W72, and 72-h averaged 10 m wind speed during the 72 h the cyclone is linked to the largest number of events for the categories (g) P72 and (h) W72. Wind composites show the mean across all extreme hazard cyclones, precipitation composites show the 95$^{\text{th}}$ percentile to account for the larger spatial variability of frontal precipitation. Solid contours indicate SLP (contours every 10 hPa), and hatched regions in (a, d, e, h) mark areas where more than 10% of cyclones are linked to an extreme of the respective category. Insets show the locations of the cyclone center at the time considered for the composite.

which identified the cold conveyor belt, convection along the cold front, and the cold sector as regions with strong winds at the time of maximum intensity of the cyclone. W1 extremes in the region where the warm conveyor belt begins its ascent are less prominent in our analysis than in Eisenstein et al. (2023), who identified this area as the dominant region for surface wind extremes in the two days prior to minimum SLP. In P1 extreme hazard cyclones, surface winds are weaker and the location of their maximum is shifted to the east compared to the winds in category W1 (Fig. 6c, d).

The locations of long-duration extremes are more spatially dispersed than those of short-duration extremes. This stems from the movement of the cyclone during the 72-h period, which causes the cyclone-relative occurrence of extremes to cover a

https://doi.org/10.5194/egusphere-2026-4755
Preprint. Discussion started: 1 September 2026

broader area. The cyclone-relative regions experiencing most of the precipitation in the P72 extreme hazard cyclones show a similar spatial pattern as the ones of the P1 cyclones, with the 95$^{\text{th}}$ percentile exceeding $170\,\mathrm{mm}$ of precipitation in the 72-h period just northeast of the center of the cyclone (Fig. 6e). As the cyclone moves during the 72-h period, precipitation associated with the cold front appears less distinct in the P72 composites than in the P1 composites. Cyclone propagation is also reflected in the southwest–northeast orientation of the precipitation pattern south of the center. The accumulated precipitation is much lower in the W72 category, with values below $65\,\mathrm{mm}$ in the 72-h period (Fig. 6f). Strong winds and W72 extremes occur in the same cyclone-relative region as in the W1 category, but, as for the precipitation extremes, their locations are more broadly distributed (Fig. 6g). Because winds are averaged over the full duration of the extreme, mean values are lower than in W1 cyclones and do not exceed $18\,\mathrm{m\,s^{-1}}$. For P72 extreme hazard cyclones, we only find weak surface winds sustained over an extended period (Fig. 6h). The striking differences in Fig. 6e, f, and Fig. 6g, h, indicate that cyclones associated with P72 extremes are most likely distinct from those associated with W72 extremes, which agrees with the low values of "overlap" between the two categories in Fig. 3.

4.2.2 PV structure and ambient winds of extreme hazard cyclones

At the time when extreme hazard cyclones are linked to the largest number of extremes in their respective category, they are characterized by positive PV anomalies extending through the full depth of the troposphere. Figure 7 shows composites of zonal vertical cross-sections for the four hazard categories at these times. All categories exhibit a PV maximum in the lower troposphere, which is more pronounced for short-duration than long-duration extremes. Maxima reach $3.6\,\mathrm{pvu}$ for P1 cyclones (Fig. 7a) and $3.3\,\mathrm{pvu}$ for W1 cyclones (Fig. 7b), compared to $3.2\,\mathrm{pvu}$ for P72 cyclones (Fig. 7c) and $1.8\,\mathrm{pvu}$ for W72 cyclones (Fig. 7d). The precipitation categories exhibit generally larger PV values than the wind categories, particularly in the lower troposphere, possibly due to enhanced diabatic PV production during condensation (e.g., Binder et al., 2016). In both precipitation categories, PV values exceeding $2\,\mathrm{pvu}$ extend from the lower to the upper troposphere, forming a vertically coherent PV tower (Fig. 7a,c), which is typical for deep extratropical cyclones (e.g., Čampa and Wernli, 2012; Wernli and Gray, 2024). In contrast, W1 cyclones exhibit mid-tropospheric PV values below $2\,\mathrm{pvu}$, while the W72 composite does not exceed $2\,\mathrm{pvu}$ below $400\,\mathrm{hPa}$, indicating that these cyclones are, compared to the other categories of extreme hazard cyclones, much less driven by diabatic PV production in the lower troposphere. This is remarkable as these cyclones are on average deeper and have stronger 24-h deepening than for instance P72 hazard cyclones, as shown previously in Fig. 5f, g.

A possible explanation for the weaker PV anomalies in the composite of W72 cyclones might be cyclone clustering, whereby multiple systems pass over the same region within the 72-h window. Although extreme hazard cyclones are identified based on their associated number of extremes, individual extreme events may be linked to more than one cyclone. Widespread extreme events are therefore not necessarily associated with a single dominant cyclone, but potentially with a sequence of systems that collectively maintain cyclonic influence over an extended period. This is reflected in the average number of cyclones passing over a grid point during the 72-h periods when most W72 extremes occur, with values of up to 1.99 cyclones over the considered grid points (not shown). A similar effect is found for P72 events, for which up to 1.74 cyclones pass over the region during the $72\,\mathrm{h}$ with the most extremes (not shown), suggesting that clustering also contributes to precipitation extremes, albeit to a

https://doi.org/10.5194/egusphere-2026-4755
Preprint. Discussion started: 1 September 2026

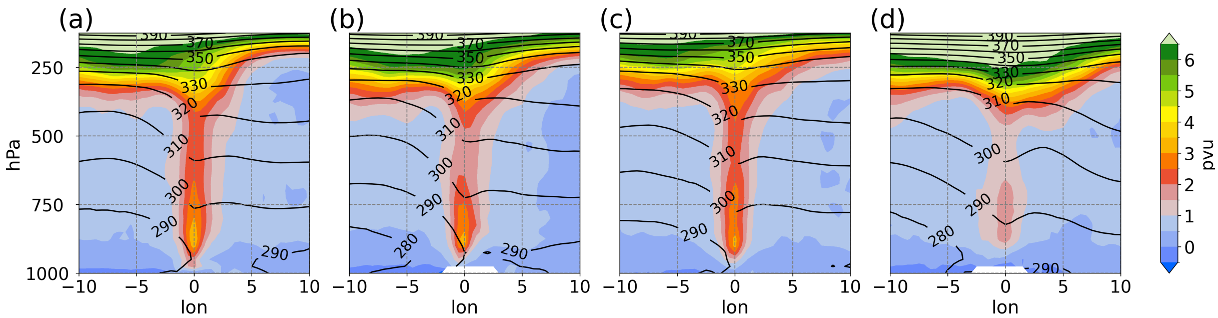

Figure 7. PV composites of zonal vertical cross-sections of extreme hazard cyclones at the time when they are linked to the largest number of extremes in the categories (a) P1, (b) W1, (c) P72, and (d) W72. Solid black contours show isentropes in 10 K increments.

lesser extent than for W72 extremes. It is therefore unlikely that this clustering effect alone explains the diagnosed differences in the PV structure of the associated cyclones and we learn more about the differing cyclone properties from now considering composites of the upper-level flow associated with the different hazard cyclone categories.

Figure 8 shows composites of PV anomalies and wind speed at 250 hPa, and the stationarity of extreme hazard cyclones, again at the time with the largest number of associated extremes. All four hazard categories are associated with pronounced positive PV anomalies at 250 hPa (8a-d). Anomalies are computed relative to a grid-point-specific 15-day running mean over the entire investigated period (March 1950 to March 2025). The magnitude of the positive PV anomalies is larger for wind extremes than for precipitation extremes, reaching peak values of 3.12 pvu for P1 (Fig. 8a), 3.64 pvu for W1 (Fig. 8b), 2.59 pvu for P72 (Fig. 8c), and 4.26 pvu for W72 extreme hazard cyclones (Fig. 8d), which are located just southwest of the cyclone center. For the 1-h categories, positive PV anomalies extend northward from the cyclone center (Fig. 8a, b). In contrast, positive PV anomalies in the 72-h categories at the same pressure level are surrounded by negative PV anomalies (Fig. 8c, d). This suggests that extremes of varying duration occur in different phases of the Rossby wave-breaking cycle, with short-duration events more likely linked to cyclones with an upper-level PV streamer, and long-duration events occurring later in the cyclone's lifetime when the PV field evolved into a structure resembling a PV cutoff, although there is some case-to-case variability.

Extreme hazard cyclones in the W1 and W72 categories are typically located in regions with strong upper-level winds near the left exit of a jet streak (Fig. 8f, h), indicating that a strong circulation in the entire troposphere and strong baroclinicity are important for wind extremes to develop. The jet is generally stronger for W72 extremes than for W1 extremes, reaching values beyond 60 $\mathrm{m\,s^{-1}}$, which may favor cyclone clustering and the passage of multiple cyclones within a relatively short time period, as discussed above. Strong upper-level winds in intense cyclones were also found by Dolores-Tesillos et al. (2022), although the maximum wind speed in their composites was located further east. For P1 and P72 cyclones, upper-level winds are weaker than for their W1 and W72 counterparts at the times linked to the highest number of extremes, with the average jet not exceeding 45 $\mathrm{m\,s^{-1}}$ for P1 (Fig. 8e) and 40 $\mathrm{m\,s^{-1}}$ for P72 (Fig. 8g). Part of this signal may also reflect the geographic distribution of the extreme hazard cyclones at their most extreme time steps: W1 and W72 extremes tend to occur closer to

https://doi.org/10.5194/egusphere-2026-4755
Preprint. Discussion started: 1 September 2026

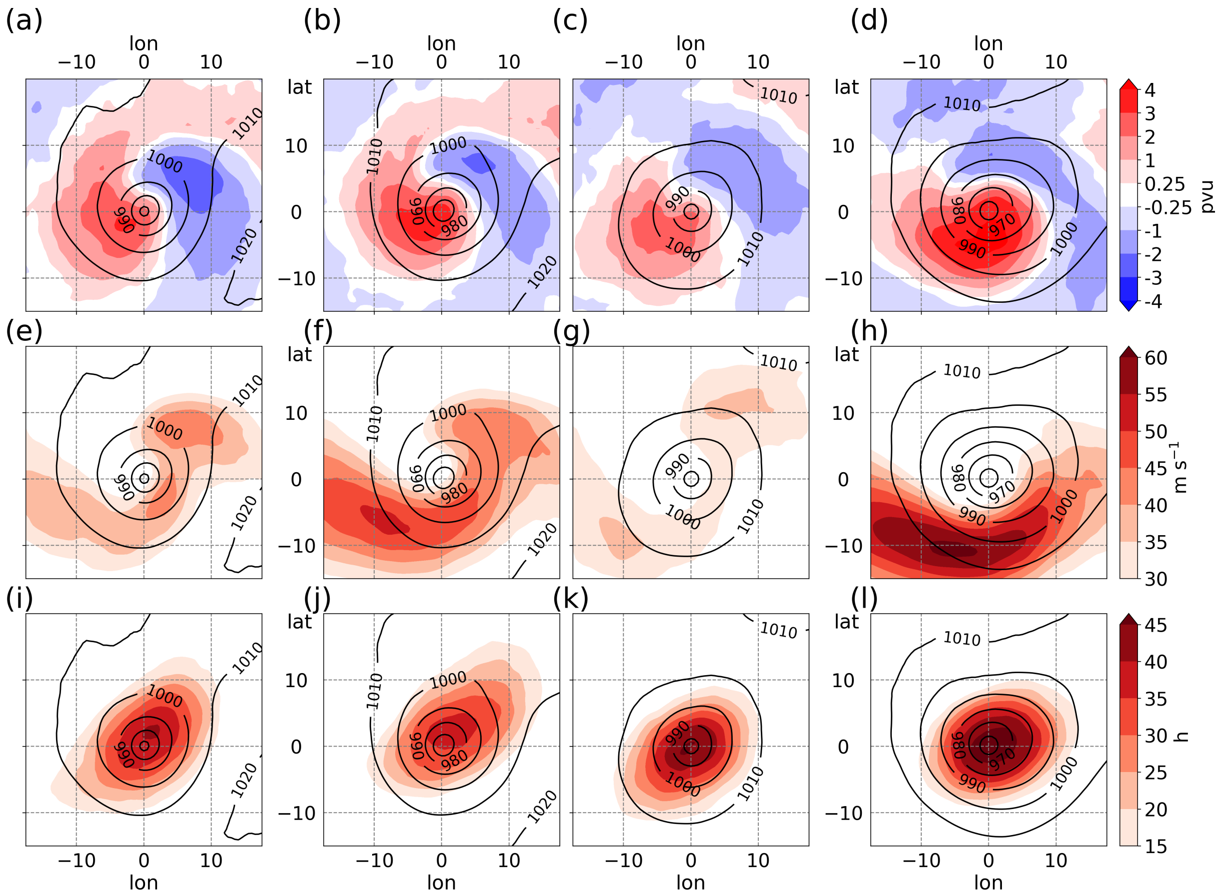

Figure 8. Cyclone-center-relative composites at the time when the extreme hazard cyclones are associated with most extremes for P1 (first column), W1 (second column), P72 (third column) and W72 (fourth column). (a–d) PV anomalies at 250 hPa relative to a 15-day running mean background, (e-h) wind speeds at 250 hPa, and (i-l) duration that cyclones cover grid points around the cyclone center at the time with the largest number of extremes. Solid black contours show SLP with 10 hPa intervals.

the US east coast, where the climatological jet is stronger compared to the central North Atlantic (e.g., Koch et al., 2006). Combined with the results of the PV cross-sections, a plausible interpretation is that P72 cyclones are strongly diabatic but develop in moderate baroclinicity, whereas for W72 cyclones baroclinicity and dry dynamical intensification are particularly strong.

4.2.3 Considerations of cyclone stationarity

Cyclone stationarity, measured as the number of hours a grid point remains within a cyclone mask, also differentiates long- from short-duration extremes. Figures 8i-l show the average duration a cyclone is located over the region where most extremes occurred. For each composited cyclone, we determine its location during that time and then quantify the number of hours the

https://doi.org/10.5194/egusphere-2026-4755
Preprint. Discussion started: 1 September 2026

cyclone area covered the surrounding grid points. For 1-h extremes, extreme hazard cyclones typically pass over a given region in about 1.5 days for the category P1 (Fig. 8i) and slightly faster for W1 (Fig. 8j). In contrast, 72-h extremes are associated with more stationary cyclones, with both categories P72 (Fig. 8k) and W72 (Fig. 8l) covering the affected regions for up to 2 days on average. The ellipsoidal shapes of constant stationarity values also indicate the typical southwest to northeast track of the cyclones. While cyclones linked to 72-h events are more stationary, the larger values seen may also be influenced by the cyclone's larger surface area in the P72 and W72 categories compared to the ones associated with 1-h extremes.

Overall, the composites highlight that P1 and W1 extremes tend to be associated with streamer-like upper-level PV structures and relatively fast-moving cyclones, whereas P72 and W72 extremes tend to occur when there is already an upper-level PV cutoff. For these long-duration extremes, the associated cyclones are either more stationary than those linked to short-duration extremes, or multiple cyclones pass through the region within the 72-h window.

4.3 Cyclone phase space during extreme events

Extreme hazard cyclones were shown to develop at more equatorward latitudes than ordinary cyclones, with some of them having cyclogenesis in the tropics and later transitioning into extratropical cyclones. The CPS has been used extensively to identify tropical cyclones undergoing extratropical transition and to describe their thermal structure. Here, we analyze extreme hazard cyclones in the P1 and W1 categories in the North Atlantic during the times they are linked to P1 and W1 extremes using the CPS. All extremes considered occur in the extratropics at latitudes poleward of 30° N. The associated cyclones are therefore expected to be strictly extratropical based on their location at the time when they are linked to the extreme event. Previous studies have referred to cyclones as tropical, extratropical, or hybrid systems based on their position in the CPS. In this study, we label the quadrants in the CPS according to their structural characteristics as 'symmetric, deep warm core' (traditionally 'tropical'; $B < 10$, $-V_T^L > 0$, and $-V_T^U > 0$), 'asymmetric, deep cold core', (traditionally 'extratropical'; $B > 10$, $-V_T^L < 0$, and $-V_T^U < 0$), 'symmetric, deep cold core', (traditionally 'decaying extratropical'; $B < 10$, $-V_T^L < 0$, and $-V_T^U < 0$), and 'symmetric, shallow warm core' (traditionally 'hybrid' or 'warm-seclusion'; $-V_T^L > 0$, and $-V_T^U < 0$). For the computation of a climatology of North Atlantic cyclones in the CPS phase space, a cyclone is included if its mask intersects the North Atlantic domain at least once at any point in its lifetime.

Figure 9 shows the distribution of extreme hazard cyclones in the CPS at times when they are associated with extreme events together with the climatology of all North Atlantic cyclones. The climatological cyclone in the North Atlantic forms as an asymmetric system with a deep cold core and becomes more symmetric over the course of its life cycle, but in most cases remains cold core. Extreme hazard cyclones in the P1 (Fig. 9a) and W1 (Fig. 9b) categories likewise have cyclogenesis as asymmetric systems with a cold core in the lower troposphere, but subsequently evolve into more symmetric cyclones with a warm core at lower levels. The majority of extreme events linked to these cyclones occur during this phase, within the symmetric warm core quadrant of the CPS.

The second type of CPS shows that the climatological cyclone in the North Atlantic has mainly a cold core extending throughout the entire troposphere. P1 extreme hazard cyclones exhibit a modest shift toward the warm core side of the diagram and an increased likelihood of developing a deep warm core compared to climatology (Fig. 9c). This structural transition is far

https://doi.org/10.5194/egusphere-2026-4755
Preprint. Discussion started: 1 September 2026

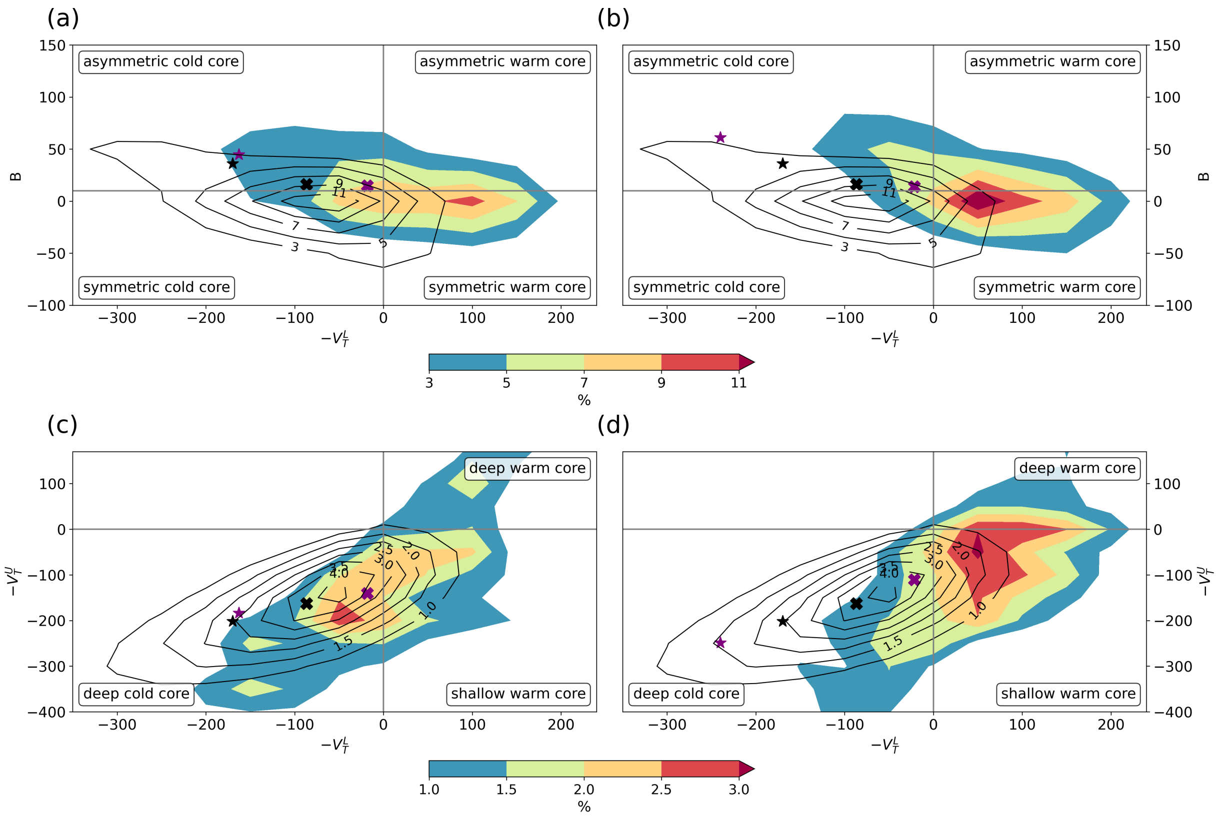

Figure 9. Cyclone phase spaces (CPS) for North Atlantic cyclones, with lower-tropospheric thermal wind $-V^LT$ and thermal asymmetry B for the top 100 **(a)** P1 and **(b)** W1 extreme hazard cyclones, and lower- and upper-tropospheric thermal wind ($-V^LT$ and $-V_T^U$), again for **(c)** P1 and **(d)** W1 extreme hazard cyclones. Shading shows the distribution in the CPS at times when extreme events of a certain type are associated with the extreme hazard cyclones, weighted by the number of extremes associated with each time step, while black contours denote the climatological distribution (showing all time steps along the tracks without weighting). Purple and black stars indicate the mean position in the CPS at cyclogenesis for extreme hazard cyclones and climatology, respectively, and purple and black crosses show the corresponding mean positions at cyclolysis.

more pronounced for W1 extreme hazard cyclones (Fig. 9d). While these systems have a deep cold core during cyclogenesis, they typically develop a shallow warm core by the time they are linked to W1 extremes.

While extreme hazard cyclones in the North Atlantic in most cases form as asymmetric systems with a deep cold core, they become more symmetric as they intensify and develop a shallow warm core, particularly the cyclones linked to many surface wind extremes. Given that all cyclones considered here are extratropical, their location in the 'symmetric, shallow warm core' quadrant of the CPS suggests that extreme hazard cyclones in the North Atlantic are Shapiro-Keyser cyclones developing a warm seclusion (Shapiro and Keyser, 1990). Extratropical cyclones with characteristics following the Shapiro-Keyser model have been linked to a wide range of surface impacts, especially impacts related to wind extremes. In this context, Gray et al.

https://doi.org/10.5194/egusphere-2026-4755
Preprint. Discussion started: 1 September 2026

(2024) showed that the majority of the most intense cyclones in terms of maximum 850 hPa relative vorticity in the mid-latitudes develop a warm seclusion and therefore also a warm core. These cyclones have also been shown to cause the strongest surface winds in western Europe (Baatsen et al., 2015) and to reach the highest intensities (in terms of minimum SLP) and near-surface wind speeds (Dekker et al., 2018). Some of these high wind speeds may be related to sting jets, which encircle the seclusion of warm air (Browning, 2004) and were identified in some of the most intense wind storms (e.g., Grønås, 1995; Browning, 2005; Parton et al., 2009; Volonté et al., 2018; Volonté and Riboldi, 2024). However, sting jets are most likely not fully represented in the ERA5 data due to insufficient resolution (Gray et al., 2024).

While the classical CPS was designed primarily to detect extratropical transitions, Besson et al. (2026) recently developed an alternative phase space specifically for cyclones in the mid-latitudes based on thermal asymmetry, the baroclinic conversion rate, and the temperature difference between the cyclone center and a 5° surrounding radius at 750 hPa. Using this phase space, they found that most extratropical cyclones in the Northern Hemisphere are asymmetric and have a warm core, and that wintertime systems with a lower-tropospheric warm core are more intense in terms of minimum SLP than cold core cyclones. Although the phase space in Besson et al. (2026) is formulated differently from the classical definition used here, our results broadly align with those from Besson et al. (2026) in that surface extremes and maximum cyclone intensity predominantly occur during the warm core phase. However, while cyclones at the time of minimum SLP are found to be relatively asymmetric by Besson et al. (2026), the top 100 extreme hazards cyclones are mostly classified as symmetric in the classical CPS at times when they are linked to surface extremes. Nevertheless, a parallel remains between the two frameworks: the mean trajectory of cold core cyclones in the Besson et al. (2026) phase space reaches its most symmetric point at minimum SLP, which is when the cyclones are also most likely linked to surface weather extremes.

5 Summary and conclusion

Using 75 years of ERA5 reanalyses, we investigated the properties of cyclones that cause a particularly high number of precipitation and 10 m wind speed extremes along their tracks, thereby posing a significant hazard to the regions they traverse. We therefore refer to these cyclones as “extreme hazard cyclones”. Precipitation and wind extremes were identified on time scales of 1 h and 72 h based on the local 99.9^{th} percentile and we linked them to cyclones if they were covered by a two-dimensional cyclone mask (at least once for the long-duration extremes). The number of local wind and precipitation extremes accumulated along each cyclone track was then quantified globally, and cyclones were ranked by their number of associated extremes, thereby identifying the most extreme cyclones in the hazard categories hourly precipitation (P1), hourly 10 m wind speed (W1), 72-h precipitation (P72), and 72-h 10 m wind speed (W72). The aims of the study are to introduce this approach and to provide a global characterization of extreme hazard cyclones. A more regional investigation of extreme hazard cyclones in the North Atlantic compares them across the four hazard categories, as well as against climatology. The main findings addressing the research questions posed in the Introduction can be summarized as follows.

1. Which cyclones accumulate the largest number of precipitation and surface wind speed extremes along their track? How do they compare to climatology in terms of their genesis location, size, intensity, intensification, thermal or PV structure?

https://doi.org/10.5194/egusphere-2026-4755
Preprint. Discussion started: 1 September 2026

The cyclones accumulating the highest number of precipitation and wind extremes are predominantly tropical systems that recurve, undergo extratropical transition, and re-intensify as extratropical cyclones. They therefore have long lifetimes, travel extensive distances, and cover large surface areas. Compared to the cyclone climatology in the extratropics, these cyclones form at lower latitudes, show stronger intensification and reach lower minimum SLP. Most extreme hazard cyclones develop strong upper-level PV anomalies, which vertically align with diabatically produced low-level PV and form a PV tower. The exception are cyclones associated with W72 extremes, which form much weaker PV towers. In the classical cyclone phase space, P1 and W1 extreme hazard cyclones are more symmetric than climatological cyclones.

2. When and where do these cyclones form? Is there a preferred season for their occurrence?

   Globally, extreme hazard cyclones form and intensify over the ocean, predominantly during local summer and autumn. In the Northern Hemisphere, they occur in the Atlantic and Pacific, while in the Southern Hemisphere, most of them form in the Pacific and Indian Ocean. A notable exception occurs in the South Atlantic, where W1 extreme hazard cyclones also form during austral winter and spring.

3. Do cyclones associated with a large number of precipitation extremes show different properties than cyclones linked to many wind extremes?

   Cyclones linked to many surface wind extremes reach lower minimum SLP and intensify more rapidly than those linked to precipitation extremes. In the extratropics, they occur in an environment with a strong upper-level jet and consequently high baroclinicity, and often develop a shallow warm core (again using the classical cyclone phase space terminology), whereas cyclones linked to many precipitation extremes strongly depend on a large supply of moisture and are associated with both deep cold core and shallow warm core systems.

4. Do cyclones linked to short-duration extremes show other characteristics than cyclones associated with longer-duration extremes?

   Cyclones linked to 1-h extremes generally reach lower minimum SLP. The largest number of 1-h extremes coincide with streamer-like structures in the upper-level PV field, whereas 72-h events are most frequent when the upper-level PV pattern already exhibits a cutoff. Long-duration events are driven either by more stationary cyclones or by cyclone clustering.

Consequently, cyclones that accumulate a large number of surface extremes do not represent a homogeneous group. Instead, they exhibit nuanced yet critical differences in their structure, life cycle, and geographical distribution, depending strongly on the specific type and duration of the hazard they are linked to. Quantifying when, where, and which characteristics each type of extreme hazard cyclone develops has crucial implications especially for civil protection and emergency management, where earlier and more precise forecasts of high-impact weather events are of utmost importance, but also for the insurance and financial sectors. Given this potential socioeconomic relevance, the methodological caveats of our approach deserve careful attention. They relate, first, to the choice of the underlying data set. We used ERA5 reanalyses to identify cyclones and surface weather extremes. While we have high confidence in the accuracy of SLP fields to capture major cyclones, there are

https://doi.org/10.5194/egusphere-2026-4755
Preprint. Discussion started: 1 September 2026

certainly limitations in the representation of surface weather extremes in ERA5. However, although regionally (over land) better datasets are available, such a global analysis over 75 years is currently only possible when using reanalysis datasets like ERA5. A second caveat concerns the cyclone tracking, which is an essential element in identifying extreme hazard cyclones. The intercomparison study by Neu et al. (2013) revealed large differences in cyclone track climatologies when using different tracking methods – but it also found that tracking is most robust against methodological choices for intense cyclones. This provides confidence in our results as extreme hazard cyclones are particularly deep and strongly intensifying (Fig. 5f, g). An important third caveat is that this study focuses strictly on hazards rather than impacts. It could be argued that several of the identified extreme hazard cyclones are not particularly relevant from a socioeconomic point of view, as they created surface weather extremes mainly over the oceans. While this is true, we consider the methodological approach of identifying extreme hazard cyclones as original and versatile, such that a stakeholder with a particular exposure field could rank cyclones according to the occurrence of surface weather extremes in regions of exposure. This would lead to the identification of extreme impact cyclones, whereas "impact" would be understood as a stakeholder-specific concept.

As an outlook, we plan to extend the methodology introduced in this study to climate model simulations. Such an analysis enables evaluating potential changes in the properties of extreme hazard cyclones, as well as variations in their preferred regions of occurrence, over the course of the 21st century under a warming climate.

Code and data availability. The ERA5 reanalysis data is openly available on the Copernicus Climate Change Service, Climate Data Store: https://doi.org/10.24381/cds.143582cf (Hersbach et al., 2023). Key cyclone track data and extreme event locations will be made available in the ETH research collection upon acceptance of the paper.

Author contributions. SV performed the research and wrote the manuscript. All authors contributed to the design of the study, discussed intermediate results, and commented previous versions of the manuscript.

Competing interests. At least one of the (co-)authors is a member of the editorial board of *Weather and Climate Dynamics*. The authors declare that they have no other competing interests.

Acknowledgements. SV and SH have been supported by the Schweizerischer Nationalfonds zur Förderung der Wissenschaftlichen Forschung (grant no. 228019). HW is grateful to Christian Grams for his unpublished work about extreme hazard cyclones about ten years ago, which was an important source of inspiration for this project.

https://doi.org/10.5194/egusphere-2026-4755
Preprint. Discussion started: 1 September 2026

References

Baatsen, M., Haarsma, R. J., Van Delden, A. J., and De Vries, H.: Severe autumn storms in future western Europe with a warmer Atlantic ocean, Clim. Dynam., 45, 949–964, https://doi.org/10.1007/s00382-014-2329-8, 2015.

Bentley, A. M., Bosart, L. F., and Keyser, D.: A climatology of extratropical cyclones leading to extreme weather events over central and eastern North America, Mon. Weather Rev., 147, 1471–1490, https://doi.org/10.1175/MWR-D-18-0453.1, 2019.

Berg, R. J. and Avila, L. A.: Atlantic hurricane season of 2009, Mon. Weather Rev., 139, 1049–1069, https://doi.org/10.1175/2010MWR3476.1, 2011.

Besson, M., Rivière, G., and Fromang, S.: A cyclone phase space dedicated to extratropical cyclones, Weather Clim. Dynam., 7, 805–823, https://doi.org/10.5194/wcd-7-805-2026, 2026.

Bieli, M., Camargo, S. J., Sobel, A. H., Evans, J. L., and Hall, T.: A global climatology of extratropical transition. Part I: characteristics across basins, J. Climate, 32, 3557–3582, https://doi.org/10.1175/JCLI-D-17-0518.1, 2019.

Binder, H., Boettcher, M., Joos, H., and Wernli, H.: The role of warm conveyor belts for the intensification of extratropical cyclones in Northern Hemisphere winter, J. Atmos. Sci., 73, 3997–4020, https://doi.org/10.1175/JAS-D-15-0302.1, 2016.

Breugem, A., Wesseling, J., Oostindie, K., and Ritsema, C.: Meteorological aspects of heavy precipitation in relation to floods – an overview, Earth Sci. Rev., 204, 103 171, https://doi.org/10.1016/j.earscirev.2020.103171, 2020.

Browning, K. A.: The sting at the end of the tail: damaging winds associated with extratropical cyclones, Q. J. Roy. Meteor. Soc., 130, 375–399, https://doi.org/10.1256/qj.02.143, 2004.

Browning, K. A.: Observational synthesis of mesoscale structures within an explosively developing cyclone, Q. J. Roy. Meteor. Soc., 131, 603–623, https://doi.org/10.1256/qj.03.201, 2005.

Čampa, J. and Wernli, H.: A PV perspective on the vertical structure of mature midlatitude cyclones in the Northern Hemisphere, J. Atmos. Sci., 69, 725–740, https://doi.org/10.1175/JAS-D-11-050.1, 2012.

Catto, J. L. and Pfahl, S.: The importance of fronts for extreme precipitation, J. Geophys. Res.-Atmos., 118, 10 791–10 801, https://doi.org/10.1002/jgrd.50852, 2013.

Catto, J. L., Jakob, C., Berry, G., and Nicholls, N.: Relating global precipitation to atmospheric fronts, Geophys. Res. Lett., 39, L10 805, https://doi.org/10.1029/2012GL051736, 2012.

Catto, J. L., Madonna, E., Joos, H., Rudeva, I., and Simmonds, I.: Global relationship between fronts and warm conveyor belts and the impact on extreme precipitation, J. Climate, 28, 8411–8429, https://doi.org/10.1175/JCLI-D-15-0171.1, 2015.

Chandra, A. and Kumar, S.: Sea surface temperature and ocean heat content during tropical cyclones Pam (2015) and Winston (2016) in the Southwest Pacific region, Mon. Weather Rev., 149, 1173–1187, https://doi.org/10.1175/MWR-D-20-0025.1, 2021.

Clark, P. A. and Gray, S. L.: Sting jets in extratropical cyclones: a review, Q. J. Roy. Meteor. Soc., 144, 943–969, https://doi.org/10.1002/qj.3267, 2018.

Davies, P. A., McCarthy, M., Christidis, N., Dunstone, N., Fereday, D., Kendon, M., Knight, J. R., Scaife, A. A., and Sexton, D.: The wet and stormy UK winter of 2019/2020, Weather, 76, 396–402, https://doi.org/10.1002/wea.3955, 2021.

Dekker, M. M., Haarsma, R. J., Vries, H. D., Baatsen, M., and Delden, A. J. V.: Characteristics and development of European cyclones with tropical origin in reanalysis data, Clim. Dynam., 50, 445–455, https://doi.org/10.1007/s00382-017-3619-8, 2018.

Dolores-Tesillos, E., Teubler, F., and Pfahl, S.: Future changes in North Atlantic winter cyclones in CESM-LE – Part 1: cyclone intensity, potential vorticity anomalies, and horizontal wind speed, Weather Clim. Dynam., 3, 429–448, https://doi.org/10.5194/wcd-3-429-2022, 2022.

Donat, M. G., Leckebusch, G. C., Pinto, J. G., and Ulbrich, U.: Examination of wind storms over central Europe with respect to circulation weather types and NAO phases, Int. J. Climatol., 30, 1289–1300, https://doi.org/10.1002/joc.1982, 2010.

Earl, N., Dorling, S., Starks, M., and Finch, R.: Subsynoptic-scale features associated with extreme surface gusts in UK extratropical cyclone events, Geophys. Res. Lett., 44, 3932–3940, https://doi.org/10.1002/2017GL073124, 2017.

Eisenstein, L., Schulz, B., Pinto, J. G., and Knippertz, P.: Identification of high-wind features within extratropical cyclones using a probabilistic random forest – part 2: climatology over Europe, Weather Clim. Dynam., 4, 981–999, https://doi.org/10.5194/wcd-4-981-2023, 2023.

Evans, J. L. and Hart, R. E.: Objective indicators of the life cycle evolution of extratropical transition for Atlantic tropical cyclones, Mon. Weather Rev., 131, 909–925, https://doi.org/10.1175/1520-0493(2003)131<0909:OIOTLC>2.0.CO;2, 2003.

Field, P. R. and Wood, R.: Precipitation and cloud structure in midlatitude cyclones, J. Climate, 20, 233–254, https://doi.org/10.1175/JCLI3998.1, 2007.

Fink, A. H., Brücher, T., Ermert, V., Krüger, A., and Pinto, J. G.: The European storm Kyrill in January 2007: synoptic evolution, meteorological impacts and some considerations with respect to climate change, Nat. Hazards Earth Syst. Sci., 9, 405–423, https://doi.org/10.5194/nhess-9-405-2009, 2009.

Gray, S. L., Volonté, A., Martínez-Alvarado, O., and Harvey, B. J.: A global climatology of sting-jet extratropical cyclones, Weather Clim. Dynam., 5, 1523–1544, https://doi.org/10.5194/wcd-5-1523-2024, 2024.

Grønås, S.: The seclusion intensification of the New Year's day storm 1992, Tellus A, 47, 733–746, https://doi.org/10.3402/tellusa.v47i5.11571, 1995.

Gyakum, J. R.: On the evolution of the QE II storm. I: synoptic aspects, Mon. Weather Rev., 111, 1137–1155, https://doi.org/10.1175/1520-0493(1983)111<1137:OTEOTI>2.0.CO;2, 1983.

Han, G., Ma, Z., Chen, D., deYoung, B., and Chen, N.: Observing storm surges from space: hurricane Igor off Newfoundland, Sci. Rep., 2, 1010, https://doi.org/10.1038/srep01010, 2012.

Hanley, J. and Caballero, R.: The role of large-scale atmospheric flow and Rossby wave breaking in the evolution of extreme windstorms over Europe, Geophys. Res. Lett., 39, L21 708, https://doi.org/10.1029/2012GL053408, 2012.

Hart, R. E.: A cyclone phase space derived from thermal wind and thermal asymmetry, Mon. Weather Rev., 131, 585–616, https://doi.org/10.1175/1520-0493(2003)131<0585:ACPSDF>2.0.CO;2, 2003.

Hart, R. E., Evans, J. L., and Evans, C.: Synoptic composites of the extratropical transition life cycle of North Atlantic tropical cyclones: factors determining posttransition evolution, Mon. Weather Rev., 134, 553–578, https://doi.org/10.1175/MWR3082.1, 2006.

Hawcroft, M. K., Shaffrey, L. C., Hodges, K. I., and Dacre, H. F.: How much Northern Hemisphere precipitation is associated with extratropical cyclones?, Geophys. Res. Lett., 39, L24 809, https://doi.org/10.1029/2012GL053866, 2012.

Hersbach, H., Bell, B., Berrisford, P., Hirahara, S., Horányi, A., Muñoz-Sabater, J., Nicolas, J., Peubey, C., Radu, R., Schepers, D., Simmons, A., Soci, C., Abdalla, S., Abellan, X., Balsamo, G., Bechtold, P., Biavati, G., Bidlot, J., Bonavita, M., De Chiara, G., Dahlgren, P., Dee, D., Diamantakis, M., Dragani, R., Flemming, J., Forbes, R., Fuentes, M., Geer, A., Haimberger, L., Healy, S., Hogan, R. J., Hólm, E., Janisková, M., Keeley, S., Laloyaux, P., Lopez, P., Lupu, C., Radnoti, G., De Rosnay, P., Rozum, I., Vamborg, F., Villaume, S., and Thépaut, J.-N.: The ERA5 global reanalysis, Q. J. Roy. Meteor. Soc., 146, 1999–2049, https://doi.org/10.1002/qj.3803, 2020.

https://doi.org/10.5194/egusphere-2026-4755
Preprint. Discussion started: 1 September 2026

Hersbach, H., Bell, B., Berrisford, P., Hirahara, S., Horányi, A., Muñoz-Sabater, J., Nicolas, J., Peubey, C., Radu, R., Schepers, D., Simmons, A., Soci, C., Abdalla, S., Abellan, X., Balsamo, G., Bechtold, P., Biavati, G., Bidlot, J., Bonavita, M., De Chiara, G., Dahlgren, P., Dee, D., Diamantakis, M., Dragani, R., Flemming, J., Forbes, R., Fuentes, M., Geer, A., Haimberger, L., Healy, S., Hogan, R. J., Hólm, E., Janisková, M., Keeley, S., Laloyaux, P., Lopez, P., Lupu, C., Radnoti, G., De Rosnay, P., Rozum, I., Vamborg, F., Villaume, S., and Thépaut, J.-N.: Complete ERA5 from 1940: Fifth generation of ECMWF atmospheric reanalyses of the global climate, Copernicus Climate Change Service (C3S) Data Store (CDS) [data set], https://doi.org/10.24381/CDS.143582cf, 2023.

Hewson, T. D. and Neu, U.: Cyclones, windstorms and the IMILAST project, Tellus A, 67, 27 128, https://doi.org/10.3402/tellusa.v67.27128, 2015.

Hoskins, B. and Berrisford, P.: A potential vorticity perspective of the storm of 15-16 October 1987, Weather, 43, 122–129, https://doi.org/10.1002/j.1477-8696.1988.tb03890.x, 1988.

Jardine, A., Selby, K., and Higgins, D.: A multidisciplinary investigation of storms Ciara and Dennis, February 2020, Int. J. Disast. Risk Re., 90, 103 657, https://doi.org/10.1016/j.ijdrr.2023.103657, 2023.

Keller, J. H., Grams, C. M., Riemer, M., Archambault, H. M., Bosart, L., Doyle, J. D., Evans, J. L., Galarneau, T. J., Griffin, K., Harr, P. A., Kitabatake, N., McTaggart-Cowan, R., Pantillon, F., Quinting, J. F., Reynolds, C. A., Ritchie, E. A., Torn, R. D., and Zhang, F.: The extratropical transition of tropical cyclones. Part II: interaction with the midlatitude flow, downstream impacts, and implications for predictability, Mon. Weather Rev., 147, 1077–1106, https://doi.org/10.1175/MWR-D-17-0329.1, 2019.

Kitabatake, N.: Climatology of extratropical transitiont of tropical cyclones in the western North Pacific defined by using cyclone phase space, J. Meteorol. Soc. Jpn., 89, 309–325, https://doi.org/10.2151/jmsj.2011-402, 2011.

Klawa, M. and Ulbrich, U.: A model for the estimation of storm losses and the identification of severe winter storms in Germany, Nat. Hazards Earth Syst. Sci., 3, 725–732, https://doi.org/10.5194/nhess-3-725-2003, 2003.

Klein, P. M., Harr, P. A., and Elsberry, R. L.: Extratropical transition of western North Pacific tropical cyclones: an overview and conceptual model of the transformation stage, Weather Forecast., 15, 373–395, https://doi.org/10.1175/1520-0434(2000)015<0373:ETOWNP>2.0.CO;2, 2000.

Koch, P., Wernli, H., and Davies, H. C.: An event-based jet-stream climatology and typology, Int. J. Climatol., 26, 283–301, https://doi.org/10.1002/joc.1255, 2006.

Kuo, Y.-H. and Reed, R. J.: Numerical simulation of an explosively deepening cyclone in the eastern Pacific, Mon. Weather Rev., 116, 2081–2105, https://doi.org/10.1175/1520-0493(1988)116<2081:NSOAED>2.0.CO;2, 1988.

Leckebusch, G. C., Ulbrich, U., Fröhlich, L., and Pinto, J. G.: Property loss potentials for European midlatitude storms in a changing climate, Geophys. Res. Lett., 34, L05 703, https://doi.org/10.1029/2006GL027663, 2007.

Liberato, M. L. R., Pinto, J. G., Trigo, R. M., Ludwig, P., Ordóñez, P., Yuen, D., and Trigo, I. F.: Explosive development of winter storm Xynthia over the subtropical North Atlantic ocean, Nat. Hazards Earth Syst. Sci., 13, 2239–2251, https://doi.org/10.5194/nhess-13-2239-2013, 2013.

Little, A. S., Priestley, M. D. K., and Catto, J. L.: Future increased risk from extratropical windstorms in northern Europe, Nat. Commun., 14, 4434, https://doi.org/10.1038/s41467-023-40102-6, 2023.

Marchi, L., Borga, M., Preciso, E., and Gaume, E.: Characterisation of selected extreme flash floods in Europe and implications for flood risk management, J. Hydrol., 394, 118–133, https://doi.org/10.1016/j.jhydrol.2010.07.017, 2010.

Masson, A.: The extratropical transition of hurricane Igor and the impacts on Newfoundland, Nat. Hazards, 72, 617–632, https://doi.org/10.1007/s11069-013-1027-x, 2014.

https://doi.org/10.5194/egusphere-2026-4755
Preprint. Discussion started: 1 September 2026

Nakano, M., Kubota, H., Miyakawa, T., Nasuno, T., and Satoh, M.: Genesis of super cyclone Pam (2015): modulation of low-frequency large-scale circulations and the Madden–Julian oscillation by sea surface temperature anomalies, Mon. Weather Rev., 145, 3143–3159, https://doi.org/10.1175/MWR-D-16-0208.1, 2017.

Neu, U., Akperov, M. G., Bellenbaum, N., Benestad, R., Blender, R., Caballero, R., Cocozza, A., Dacre, H. F., Feng, Y., Fraedrich, K., Grieger, J., Gulev, S., Hanley, J., Hewson, T., Inatsu, M., Keay, K., Kew, S. F., Kindem, I., Leckebusch, G. C., Liberato, M. L. R., Lionello, P., Mokhov, I. I., Pinto, J. G., Raible, C. C., Reale, M., Rudeva, I., Schuster, M., Simmonds, I., Sinclair, M., Sprenger, M., Tilinina, N. D., Trigo, I. F., Ulbrich, S., Ulbrich, U., Wang, X. L., and Wernli, H.: IMILAST: a community effort to intercompare extratropical cyclone detection and tracking algorithms, B. Am. Meteorol. Soc., 94, 529–547, https://doi.org/10.1175/BAMS-D-11-00154.1, 2013.

Parton, G., Dore, A., and Vaughan, G.: A climatology of mid-tropospheric mesoscale strong wind events as observed by the MST radar, Aberystwyth: a climatology of mid-tropospheric mesoscale strong wind events, Meteor. Appl., 17, 340–354, https://doi.org/10.1002/met.203, 2010.

Parton, G. A., Vaughan, G., Norton, E. G., Browning, K. A., and Clark, P. A.: Wind profiler observations of a sting jet, Q. J. Roy. Meteor. Soc., 135, 663–680, https://doi.org/10.1002/qj.398, 2009.

Peijun, Z., Yongguang, Z., Chunxi, Z., and Zuyu, T.: A study of the extratropical transformation of typhoon Winnie (1997), Adv. Atmos. Sci., 22, 730–740, https://doi.org/10.1007/BF02918716, 2005.

Pezza, A. B. and Simmonds, I.: Large-scale factors in tropical and extratropical cyclone transition and extreme weather events, Ann. NY Acad. Sci., 1146, 189–211, https://doi.org/10.1196/annals.1446.005, 2008.

Pfahl, S.: Characterising the relationship between weather extremes in Europe and synoptic circulation features, Nat. Hazards Earth Syst. Sci., 14, 1461–1475, https://doi.org/10.5194/nhess-14-1461-2014, 2014.

Pfahl, S. and Sprenger, M.: On the relationship between extratropical cyclone precipitation and intensity, Geophys. Res. Lett., 43, 1752–1758, https://doi.org/10.1002/2016GL068018, 2016.

Pfahl, S. and Wernli, H.: Quantifying the relevance of cyclones for precipitation extremes, J. Climate, 25, 6770–6780, https://doi.org/10.1175/JCLI-D-11-00705.1, 2012.

Pfahl, S., Madonna, E., Boettcher, M., Joos, H., and Wernli, H.: Warm conveyor belts in the ERA-Interim dataset (1979–2010). Part II: moisture origin and relevance for precipitation, J. Climate, 27, 27–40, https://doi.org/10.1175/JCLI-D-13-00223.1, 2014.

Raveh-Rubin, S.: Dry intrusions: lagrangian climatology and dynamical impact on the planetary boundary layer, J. Climate, 30, 6661–6682, https://doi.org/10.1175/JCLI-D-16-0782.1, 2017.

Rey, T., Le De, L., Leone, F., and Gilbert, D.: An integrative approach to understand vulnerability and resilience post-disaster: the 2015 cyclone Pam in urban Vanuatu as case study, Disaster Prevention and Management: An International Journal, 26, 259–275, https://doi.org/10.1108/DPM-07-2016-0137, 2017.

Riboldi, J., Noyelle, R., Agayar, E., Binder, H., Federer, M., Hartmuth, K., Sprenger, M., Thurnherr, I., and Vishnupriya, S.: Storm Boris (2024) in the current and future climate: a dynamics-centered contextualization, and some lessons learnt, Weather Clim. Dynam., 7, 65–87, https://doi.org/10.5194/wcd-7-65-2026, 2026.

Roebber, P. J.: Statistical analysis and updated climatology of explosive cyclones, Mon. Weather Rev., 112, 1577–1589, https://doi.org/10.1175/1520-0493(1984)112<1577:SAAUCO>2.0.CO;2, 1984.

Rudeva, I. and Gulev, S. K.: Composite analysis of North Atlantic extratropical cyclones in NCEP–NCAR reanalysis data, Mon. Weather Rev., 139, 1419–1446, https://doi.org/10.1175/2010MWR3294.1, 2011.

https://doi.org/10.5194/egusphere-2026-4755
Preprint. Discussion started: 1 September 2026

Sainsbury, E. M., Schiemann, R. K. H., Hodges, K. I., Shaffrey, L. C., Baker, A. J., and Bhatia, K. T.: How important are post-tropical cyclones for European windstorm risk?, Geophys. Res. Lett., 47, e2020GL089 853, https://doi.org/10.1029/2020GL089853, 2020.

Sainsbury, E. M., Schiemann, R. K. H., Hodges, K. I., Baker, A. J., Shaffrey, L. C., and Bhatia, K. T.: Why do some post-tropical cyclones impact Europe?, Mon. Weather Rev., 150, 2553–2571, https://doi.org/10.1175/MWR-D-22-0111.1, 2022.

Salmon, E. M. and Smith, P. J.: A synoptic analysis of the 25–26 January 1978 blizzard cyclone in the central United States, B. Am. Meteorol. Soc., 61, 453–460, https://doi.org/10.1175/1520-0477(1980)061<0453:FOFASA>2.0.CO;2, 1980.

Shapiro, M. A. and Keyser, D.: Fronts, jet streams and the tropopause, in: Extratropical Cyclones, edited by Newton, C. W. and Holopainen, E. O., pp. 167–191, American Meteorological Society, ISBN 978-1-944970-33-8, https://doi.org/10.1007/978-1-944970-33-8_10, 1990.

Sprenger, M., Fragkoulidis, G., Binder, H., Croci-Maspoli, M., Graf, P., Grams, C. M., Knippertz, P., Madonna, E., Schemm, S., Škerlak, B., and Wernli, H.: Global climatologies of eulerian and lagrangian flow features based on ERA-Interim, B. Am. Meteorol. Soc., 98, 1739–1748, https://doi.org/10.1175/BAMS-D-15-00299.1, 2017.

Takemi, T.: The evolution and intensification of cyclone Pam (2015) and resulting strong winds over the southern Pacific islands, J. Wind Eng. Ind. Aerod., 182, 27–36, https://doi.org/10.1016/j.jweia.2018.09.007, 2018.

Taniguchi, K. and Tajima, Y.: Variations in extreme wave events near a South Pacific island under global warming: case study of tropical cyclone Tomas, Prog. Earth Planet Sci., 7, 8, https://doi.org/10.1186/s40645-020-0321-y, 2020.

Volonté, A. and Riboldi, J.: The origins of storm Ciarán : from diabatic Rossby wave to warm-seclusion cyclone with a sting jet, Weather, 79, 390–396, https://doi.org/10.1002/wea.7632, 2024.

Volonté, A., Clark, P. A., and Gray, S. L.: The role of mesoscale instabilities in the sting-jet dynamics of windstorm Tini, Q. J. Roy. Meteor. Soc., 144, 877–899, https://doi.org/10.1002/qj.3264, 2018.

Wernli, H. and Gray, S. L.: The importance of diabatic processes for the dynamics of synoptic-scale extratropical weather systems – a review, Weather Clim. Dynam., 5, 1299–1408, https://doi.org/10.5194/wcd-5-1299-2024, 2024.

Wernli, H. and Schwierz, C.: Surface cyclones in the ERA-40 dataset (1958–2001). Part I: novel identification method and global climatology, J. Atmos. Sci., 63, 2486–2507, https://doi.org/10.1175/JAS3766.1, 2006.

Wernli, H., Dirren, S., Liniger, M. A., and Zillig, M.: Dynamical aspects of the life cycle of the winter storm 'Lothar' (24–26 December 1999), Q. J. Roy. Meteor. Soc., 128, 405–429, https://doi.org/10.1256/003590002321042036, 2002.

Wood, K. M. and Ritchie, E. A.: A 40-year climatology of extratropical transition in the eastern North Pacific, J. Climate, 27, 5999–6015, https://doi.org/10.1175/JCLI-D-13-00645.1, 2014.

Zhang, Q., Kuo, Y., and Chen, S.: Interaction between concentric eye-walls in super typhoon Winnie (1997), Q. J. Roy. Meteor. Soc., 131, 3183–3204, https://doi.org/10.1256/qj.04.33, 2005.